6-2020

An Integrated Approach (Remote Sensing, Hydrogeology, GIS, and Statistical Modeling) to Identify the Distribution of Shallow Groundwater Occurrences over Southwest Saudi Arabia

Fahad Khudier Alshehri
Western Michigan University, Falshehri@ksu.edu.sa

AN INTEGRATED APPROACH (REMOTE SENSING, HYDROGEOLOGY, GIS, AND STATISTICAL MODELING) TO IDENTIFY THE DISTRIBUTION OF SHALLOW GROUNDWATER OCCURRENCES OVER SOUTHWEST SAUDI ARABIA

by

Fahad Khudier Alshehri

A dissertation submitted to the Graduate College
in partial fulfillment of the requirements
for the degree of Doctor of Philosophy
Geological and Environmental Sciences
Western Michigan University
June 2020

Doctoral Committee:

Mohamed Sultan, Ph.D., Chair
Matt Reeves, Ph.D.
Alan Kehew, Ph.D.
Richard Becker, Ph.D.

AN INTEGRATED APPROACH (REMOTE SENSING,HYDROGEOLOGY, GIS, AND STATISTICAL MODELING)TO IDENTIFY THE DISTRIBUTION OF SHALLOW GROUNDWATER OCCURRENCES OVER SOUTHWEST SAUDI ARABIA

Fahad Khudier Alshehri, Ph.D.

Western Michigan University, 2020

Identifying shallow (near-surface) groundwater in arid and hyper-arid areas has significant societal benefits, yet it is a costly operation when traditional methods (geophysics and drilling) are applied over large domains. In this study, we developed and successfully applied methodologies that rely heavily on readily available temporal, visible and near-infrared, radar, and thermal remote sensing data sets and field data, as well as statistical approaches to map the distribution of shallow (1–5 m deep) groundwater occurrences in Al Qunfudah Province, Saudi Arabia and to identify the factors controlling their development. A four-fold approach was adopted: (1) constructing a digital database to host relevant geologic, hydrogeologic, topographic, land use, climatic, and remote sensing data sets; (2) identifying the distribution of areas characterized by shallow groundwater levels; (3) developing conceptual and statistical models to map the distribution of shallow groundwater occurrences; and (4) constructing artificial neural network (ANN) and multivariate regression (MR) models to map the distribution of shallow groundwater, test the models over areas of known depth to groundwater (area of Al Qunfudah city and surroundings: 294 km2), and apply

the better of the two models to map the shallow groundwater occurrences across the entire Al Qunfudah Province (area: 4680 km2). Findings include: (1) high performance for the ANN (92%) and MR (88%) models in predicting the distribution of shallow groundwater using temporal-derived remote sensing products (e.g., Normalized Difference Vegetation Index [NDVI], radar backscatter coefficient, precipitation, and brightness temperature) and field data (depth to water table); (2) areas witnessing shallow groundwater levels show high NDVI (mean and standard deviation [STD]), radar backscatter coefficient values (mean and STD), and low brightness temperature (mean and STD) compared to their surroundings; (3) correlations of temporal groundwater levels and satellite-based precipitation suggest that the observed (2017–2019) rise in groundwater levels is related to an increase in precipitation in these years compared to the previous three years (2014–2016); and (4) the adopted methodologies are reliable, cost-effective, and could potentially be applied to identify shallow groundwater along the Red Sea Hills and in similar settings worldwide.

ACKNOWLEDGMENTS

First and foremost, praise and thanks to the Allah, the Almighty, for his blessings throughout my research work to complete my Ph.D. successfully.

I would like to express my deepest gratitude to my advisor Dr. Mohamed Sultan, for his encouragement, support, advice and continued help during my Ph.D. research. I want to express my gratitude also to my committee members, Dr. Matt Reeves, Dr. Alan Kehew from the Department of Geological and Environmental sciences at Western Michigan University, and Dr. Richard Becker from the University of Toledo for their valuable ideas, suggestions and constructive reviews.

In addition, I want to thank Saudi and US institutions, and their administrators for their generous support throughout my Ph.D. program. Specifically, the King Saud University, the Saudi Arabia Cultural Mission, the Saudi Geological Survey, the Ministry of Environment, Water and Agriculture in the Kingdom of Saudi Arabia and the Earth Sciences Remote Sensing Facility and the Department of Geological and Environmental Sciences at Western Michigan University.

Finally, I am extremely grateful to my parents, wife, and my son Abdulaziz for their patience, understanding, prayers and continued support. It is hard to find words to describe my appreciation and thanks to them. Thank you for shaping my life.

Fahad Khudier Alshehri

TABLE OF CONTENTS

Table of Contents—Continued

CHAPTER

Table of Contents - Continued

APPENDICES

LIST OF TABLES

LIST OF FIGURES

CHAPTER 1

INTRODUCTION

Groundwater accounts for 30.1% of the world's fresh water supplies (Peter H. Gleick, 1993). A number of natural factors (e.g., precipitation, evaporation, temperature, climate change, and aquifer properties) and anthropogenic factors (e.g., irrigation, water diversion projects, and construction of dams) affect groundwater levels, its availability and its quality (Bob, et al., 2015). In arid and semi-arid region, during wet climatic periods, fluvial systems and drainage networks develop, underlying aquifers recharge, rising groundwater tables discharge in lowlands and depressions, runoff and sediment load increase, and interactions between surface runoff and groundwater flow systems intensify. The opposite happens in dry periods, where runoff is reduced, surface drainage patterns dry up, aquifer recharge is reduced and localized, groundwater tables are lowered, and groundwater discharge decreases in lowlands (Abotalib et al., 2016). Declining groundwater levels could be related to anthropogenic factors as well, especially in areas where fossil aquifers have been mined excessively for land reclamation purposes (Motagh et al. 2007).Examples include the Mega Aquifer System (MAS) in the Arabian Peninsula (e.g., Hoetzl et al., 1978; Jado and Zötl 1984; Sultan et al., 2014), the Nubian Aquifer System in northeastern Africa (Mohamed et al. 2017), the North Western Sahara Aquifer System in north western Africa, the Great Artesian Basin in eastern Australia (Mohamed et al. 2017), and the aquifer system in northeast Iran near the city of Mashhad (Motagh et al., 2007). On the other hand, there

has been reports of rising groundwater levels in many other parts of the arid world. These reported occurrences of rising groundwater were found to be largely local in distribution and have been attributed to lack of organized discharge systems, leakages from water supply systems or from cesspools (Abu Rizaiza and Hasan, 1989), and excessive infiltration from precipitation or irrigation (e.g., Bayumi et al., 2003).

The identification of areas witnessing this phenomena has been traditionally accomplished by collecting head data from monitoring wells or by conducting near-surface geophysical methods such as electrical resistivity and ground penetrating radar, where groundwater is detected by its high conductivity and high dielectric constant compared to its surroundings (e.g., Omolaiye et al., 2011; Zawawi et al, 2014; Essam et al, 2019). Likewise, remote sensing techniques have been utilized to map shallow groundwater in discharge areas, yet the majority of these investigations focused on the use of one or two remotely acquired data sets (e.g., Hoffmann, 2005; Tweed et al, 2007; Donohue et al, 2009). For example, discharge areas and shallow groundwater were identified in Western Australia using tone variations in surface reflectance properties portrayed in Landsat Thematic Mapper (TM) false color composites and variations in surface roughness (Salama et al. 1994). Discharge areas were also identified from the high Normalized Difference Vegetation Index (NDVI) values over natural vegetation in the arid Ejina area in China (Huang et al, 2019; Jin et al., 2011) and from thermal satellite imagery given that groundwater discharge has contrasting heat signature compared to the surroundings areas (e.g., Anderson, 2005; Pfister et al., 2010; Schuetz and Weiler, 2011).

Our approach is different from the earlier attempts in two major ways: (1) we developed remote sensing-based methodologies that utilize a large number of remote sensing data sets (e.g., Moderate Resolution Imaging Spectroradiometer [MODIS] NDVI and Land Surface Temperature [LST], radar backscatter coefficient [RBC] from Sentinel-1, Soil moisture and Ocean Salinity [SMOS] measurements, Global Precipitation Measurement [GPM] and Tropical Rainfall Measuring Mission [TRMM] estimates) in conjunction with hydrogeologic information (e.g., depth to water table [DTW]), and (2) we developed statistical models that relate the observed shallow groundwater occurrences over areas where field data is available to the remotely acquired observations and use these models to predict the distribution of shallow groundwater elsewhere. The developed models are used to identify areas of shallow groundwater and to assist in the identification of the factor(s) controlling the observed rise in groundwater levels. We use Al Qunfudah city and the surrounding coastal plain in Southwest Saudi Arabia as our test site.

In this thesis, I applied an integrated approach (remote sensing, Geographic Information Systems (GIS), hydrogeology, field investigations and statistical modeling) to identify and map the distribution of shallow groundwater occurrences, and also to investigate the factor(s) controlling these phenomena across the study area. Chapter 2 describes the geologic, hydrogeologic setting of the investigated area. Chapter 3 focuses on the methodology. This includes the following tasks: (1) construct a digital database (GIS) to host relevant geologic, hydrogeologic, topographic, land

use, climatic, and remote sensing data sets, (2) develop and test a conceptual model that explains the observed spatial and temporal correlations between the individual variables and the target variable (shallow groundwater), and (3) construct and validate statistical models to map shallow groundwater occurrences using statistical models (e.g.; Multivariate Linear Regression and Artificial Neural Network). Discussion and results are given in Chapter 4 and a summary and conclusion in Chapter 5.

CHAPTER 2

GEOLOGIC, HYDROGEOLOGIC AND CLIMATIC SETTING

2.1 Introduction

In many of the arid and semi-arid regions worldwide, groundwater resources are the sole sources for fresh water supplies. Some of these valuable resources are found at shallow depths (few meters) and others at intermediate depths (say 100 to 500 m), or at deep depths (>500 m). Naturally, the shallower the groundwater, the more the cost-effective their use can be. Thus, locating these shallow water resources, especially those that occur over extensive areas could have societal benefits. On the other hand, shallow groundwater could have adverse effects as well. Rising groundwater, especially in urban areas could adversely affect the stability of buildings and structures. It could also produce adverse health impacts as well. In these cases, identifying the causes of observed rise in groundwater levels is important to mitigate this phenomena, when and where it occurs.

2.2 Geologic, Hydrogeologic, and Climatic Setting of the Investigated Area

The Red Sea Hills crop out along the Red Sea coastal plain and are composed largely of Neoproterozoic (550–900 Ma) volcano-sedimentary rock units of the Arabian–Nubian Shield in Egypt, Sudan, Ethiopia, and the Kingdom of Saudi Arabia (Sultan et al. 1990; Stern and Kroner 1993). The crystalline basement are unconformably overlain by thick sequences of sedimentary formations ranging in age

from Cambrian to Recent. The basement rocks are represented by metamorphosed volcanic and sedimentary rock associations of late Proterozoic age (Prinz, 1984). During the Miocene, northwest- trending extensional faults related to the Red Sea rifting developed and locally extrusion of basalt flows occurred in areas proximal to the Red Sea escarpment. Within the coastal plain, Quaternary coastal sediments and wadi alluvium covered the down-dropped basement complex (Prinz, 1984).

Along the eastern and western margins of the Red Sea Hills, watersheds collect precipitation from the adjoining Red Sea Hills and channel the collected runoff toward the Red Sea and its coastal plain as surface runoff and/or groundwater flow. As the runoff reaches the gently dipping coastal plain, it slows down, and deposits its sediment load. The alluvial aquifers flooring the channel networks are fed by infiltration from the runoff and by groundwater flow from the fractured basement aquifers within the Red Sea Hills (Sultan, 2008). The study area (Al Qunfudah Province) is located within the eastern coastal plain of the Red Sea in southwest Saudi Arabia and is part of the Asir mountainous region, which runs parallel to the Red Sea (Fig.1). The Asir region receives the highest average annual precipitation (AAP) in the Kingdom of Saudi Arabia (400 to 700 mm yr−1) (Sulaiman et al, 2018) (Fig.2). A number of cities are located within the Red Sea coastal plain, one of them is the major city of Al Qunfudah (area: 294 km^2) within the study area, with a population exceeding 300,000. This city is apparently built along one of the main channels draining a large (2,299 km2) watershed, the Ganunah watershed (Fig.1b). The main channels are subject to flooding

during high precipitation events (Bayumi et al, 2000) and are often the sites of organized agricultural development. The city of Al Qufudah is developed on alluvial fan deposits, where there is a 1 to 2% elevation gradient of the ground surface that increases from sea level to more than 100 m above mean sea level (a.m.s.l) within 5 to 10 km east of the Red Sea coastline (Fig.4).

Climatic conditions are necessary ingredients for any surface or groundwater resources evaluation study. The study area characterized by a semi-arid climate with occasional high intensity rainfall and rare floods leading to occasional large amount of surface water and subsequent groundwater recharge (El-Khatib, 1980). In the study area, precipitation over the adjacent Red Sea Hills is collected as surface runoff in the main channels which discharge in coastal plain and recharge the underlying thick aquifer systems.

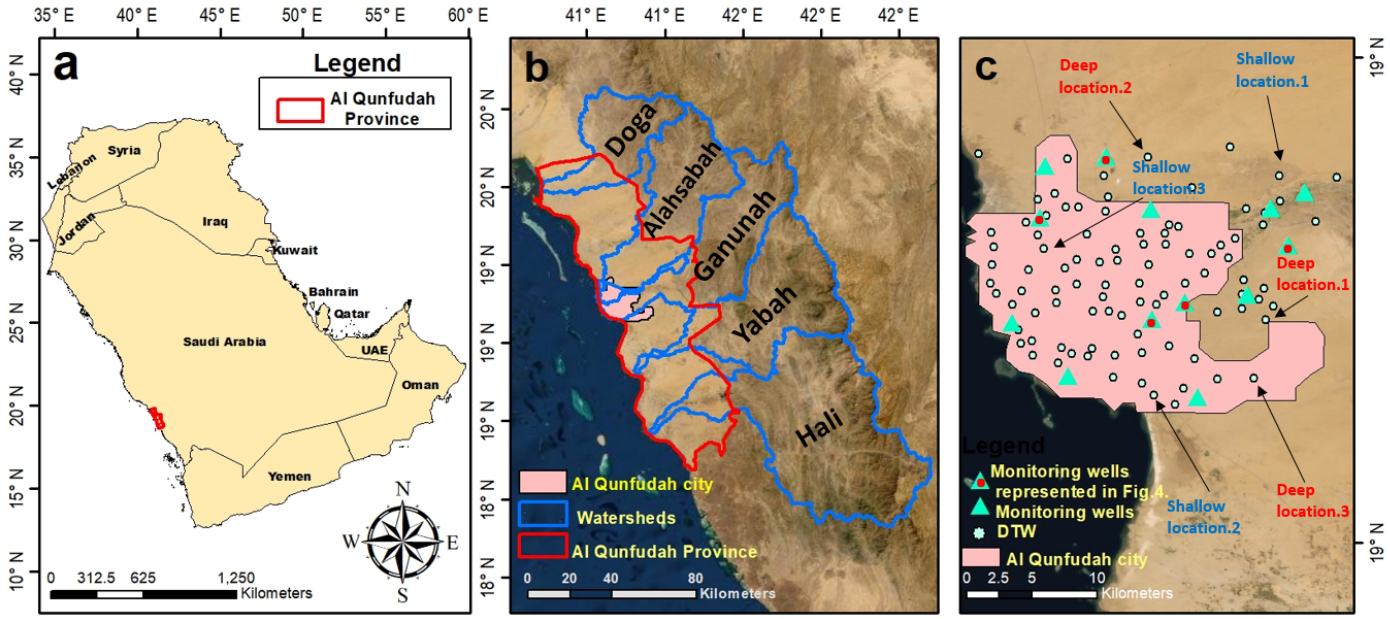

Figure 1. Location of the study area. (a) Map of the Arabian Peninsula showing the location of the study area, Al Qunfudah Province (outlined by red polygon) in southwest Saudi Arabia, (b) Extent of Al Qunfudah city, Al Qunfudah Province, Hali, Yabah, Ganunah Al ahsabah and Doga watersheds, and; (c) Zoomed-in view of Al Qunfudah city, location of monitoring wells, location of wells from which DTW were measured, and labelled location of selected wells used to test our conceptual model.

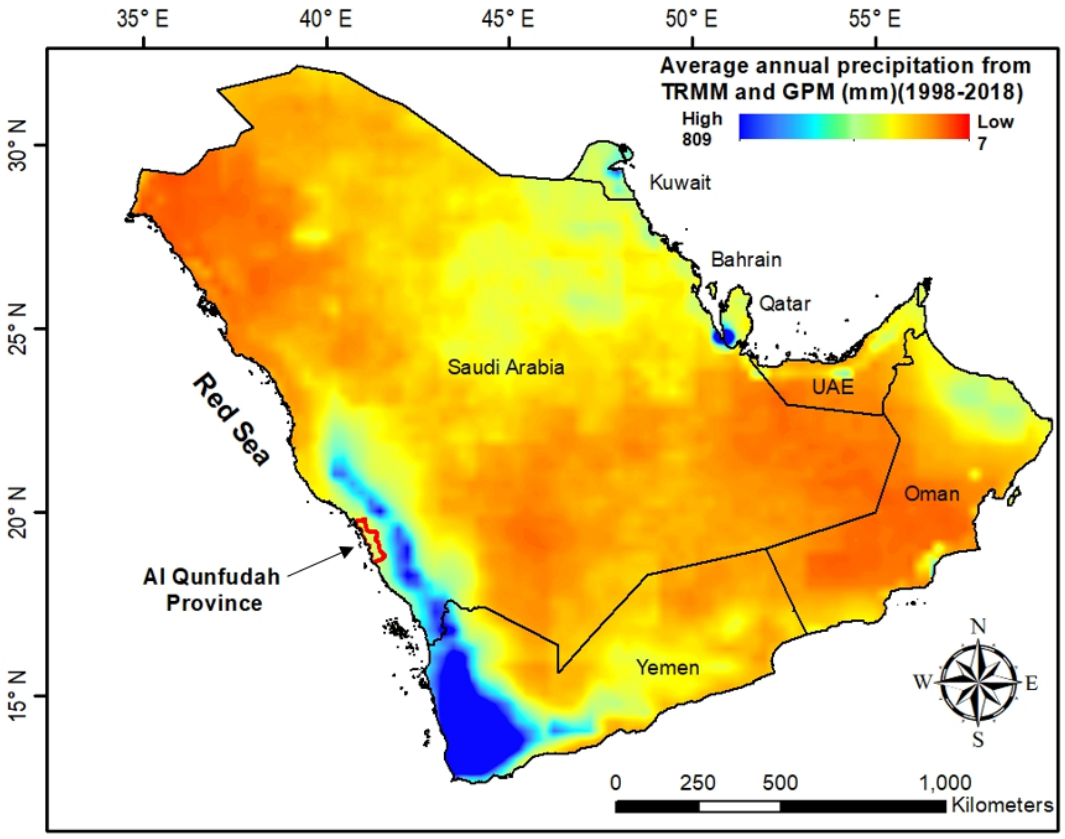

Figure 2. Average annual precipitation (AAP; 1998–2018) extracted from TRMM. (3-hourly_3B42 v7, spatial resolution: 0.25°x 0.25°) and GPM (IMERG Final Precipitation L3 0.5-hourly, spatial resolution: 0.1° x 0.1°0 V05) showing the highest regional rainfall in the southwestern part of the Arabian Peninsula including Al Qunfudah Province

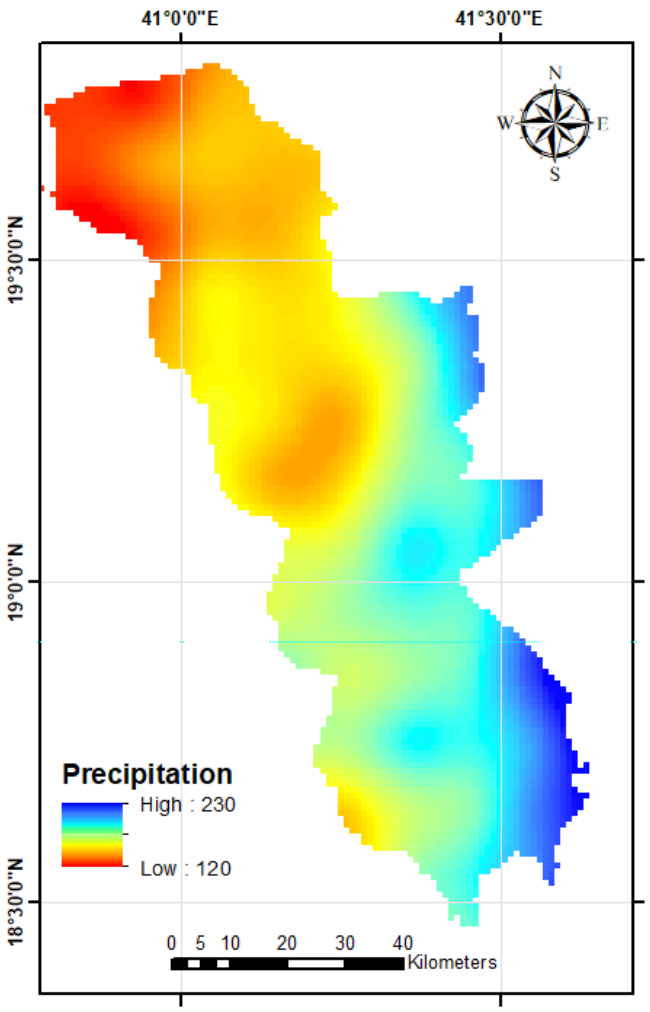

Figure 3. Average annual precipitation (AAP; 2014–2018) extracted from GPM. (IMERG Final Precipitation L3 0.5-hourly, spatial resolution: 0.1° x 0.1°0 V05) showing the average rainfall in Al Qunfudah Province.

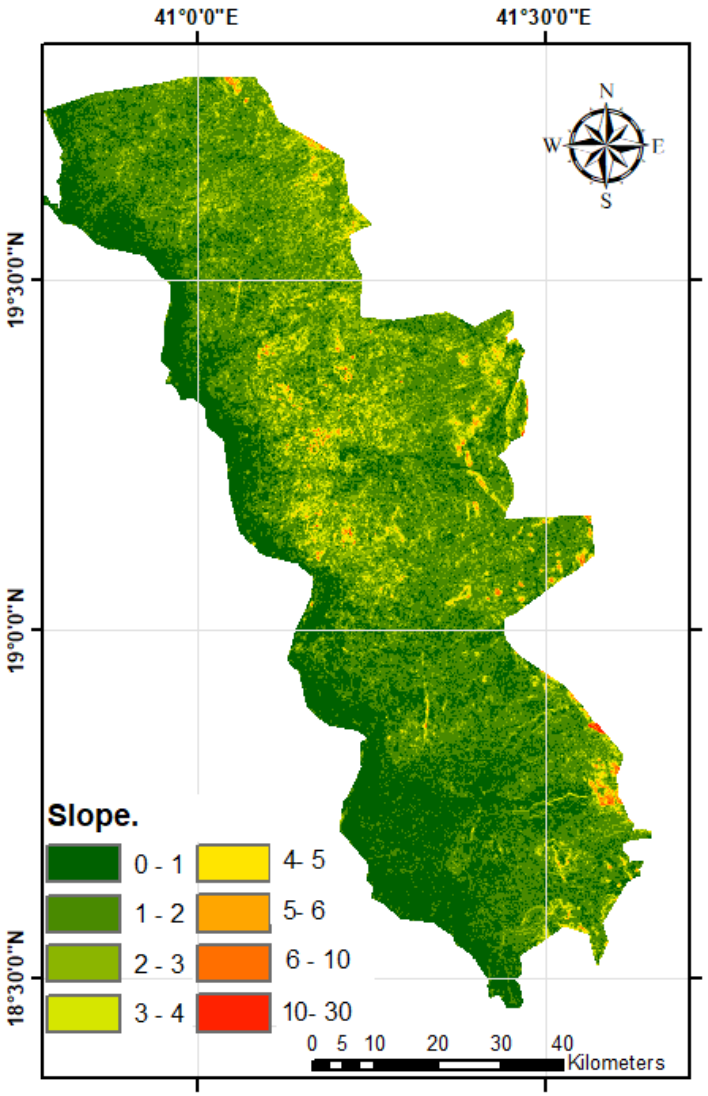

Figure 4. Slope image map of Al Qunfudah Province. Extracted from digital elevation model (DEM) using the Advanced Spaceborne Thermal Emission and Reflection Radiometer (ASTER).

CHAPTER 3

METHODOLOGY

3.1 Methods

We accomplished the goals described earlier, the identification of areas experiencing shallow groundwater and their controlling factor(s), by developing multivariate regression and Artificial Neural Networks statistical models over Al Qunfudah city and surrounding where field observations (depth to water table) are available. An inventory was compiled for reported (by the Saudi Geological Survey) occurrences of areas witnessing shallow groundwater levels in the coastal zone of Al Qunfudah. The statistical relationships relate the field observations to remotely acquired datasets. The adopted procedures involved four major steps: (1) construct a digital database (GIS) to host relevant geologic, hydrogeologic, topographic, land use, climatic, and remote sensing datasets; (2) develop and test a conceptual model that explains the observed spatial and temporal correlations between the individual variables and the target variable (shallow groundwater); (3) construct and validate statistical models to map the distribution of shallow groundwater occurrences using multivariate regression and artificial neural networks over Al Qunfudah city and surroundings; and (4) use the optimum statistical model to map the distribution of shallow groundwater occurrences across the entire Al Qunfudah Province (Fig.5). In the development of the conceptual model, we examined whether remotely acquired observations over areas characterized by shallow groundwater are different from those

acquired over deep wells. We also examined whether there are larger variations in these variables over shallow, compared to deep, groundwater areas. The remote sensing data included Normalized Different Vegetation Index (NDVI), Land Surface Temperature (LST), Soil Moisture Ocean Salinity (SMOS), Global Precipitation Measurement (GPM), Sentinel-1A Radar Backscattering Coefficient (RBC).

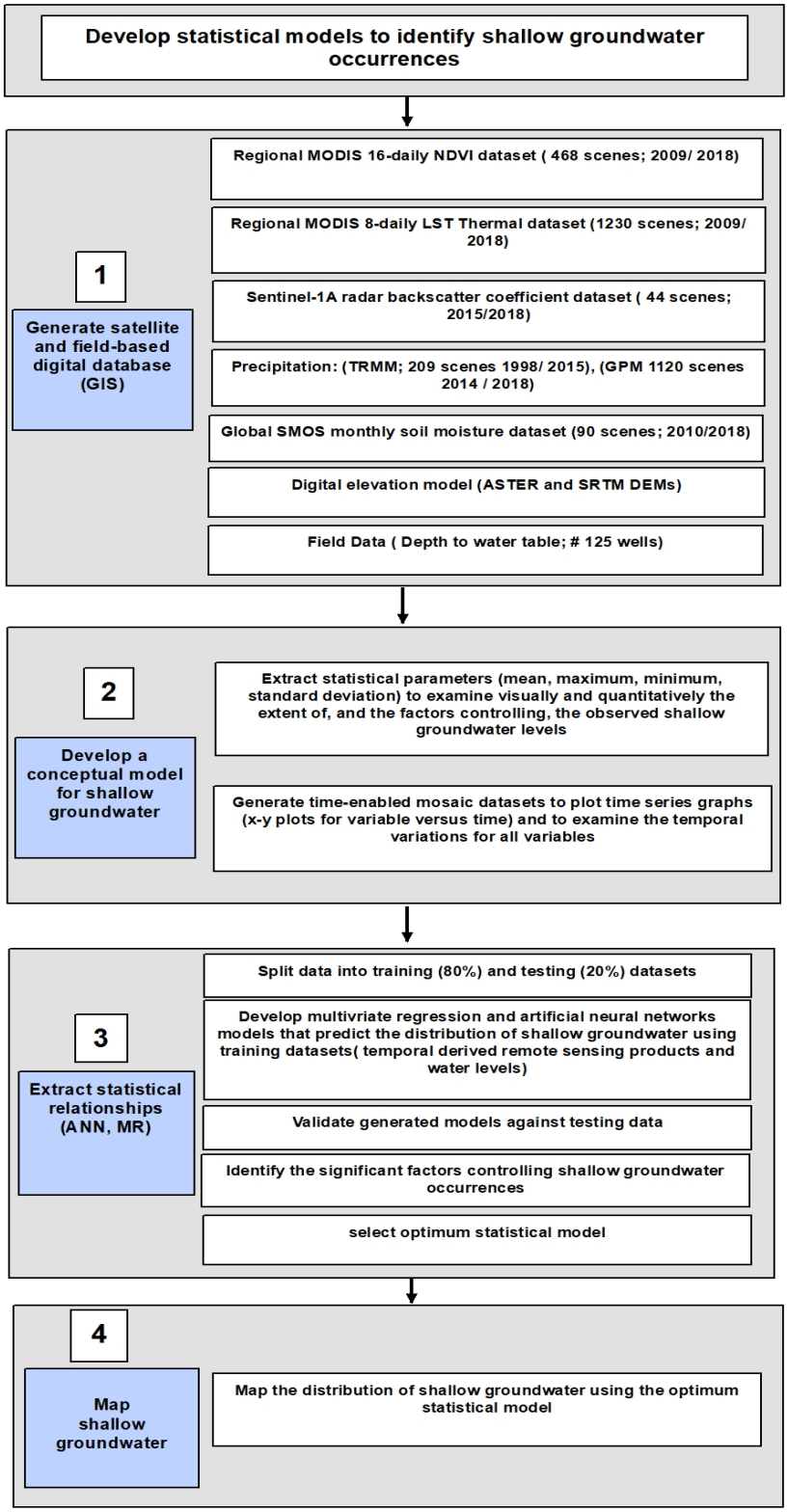

Figure 5. Four-step workflow for mapping the distribution of shallow groundwater.

3.2 Construct a digital database (GIS) to host relevant datasets

The first step involved the generation of a GIS to host all relevant datasets that could be used for the identification of areas of shallow groundwater and the factors controlling this phenomenon. These include the temporal and spatial remote sensing products and field datasets. This step involved collecting field data (e.g., DTW; number of wells: 125) and downloading and processing temporal visible and near-infrared (VNIR), thermal, radar, precipitation (GPM), and SMOS data sets to compute LST, NDVI, soil moisture, precipitation, and RBC. In this section we also explain the response of the selected remote sensing measurements in areas of shallow groundwater.

3.2.1 Identify depth to water (DTW) as target data

The Saudi Geological Survey (SGS) conducted an intensive drilling project, where 125 wells were drilled in year 2016 (FIG.4). Following the completion of the drilling project for the wells, the depth to water table was measured for each well during a period of few weeks in the months of October, and November. We classified the wells into two groups, shallow wells (≤ 5m) and deep wells (>5m). In the construction of the statistical models, the depth to water table was used as the target variable. Temporal measurements for the water table was available for a limited number of wells (13 wells), in all of which, a rise (1 to 2m) in groundwater level was reported in years

2017 to 2019 (Fig.5). Figure 4 shows the rise in groundwater levels in five of these wells over the past three years.

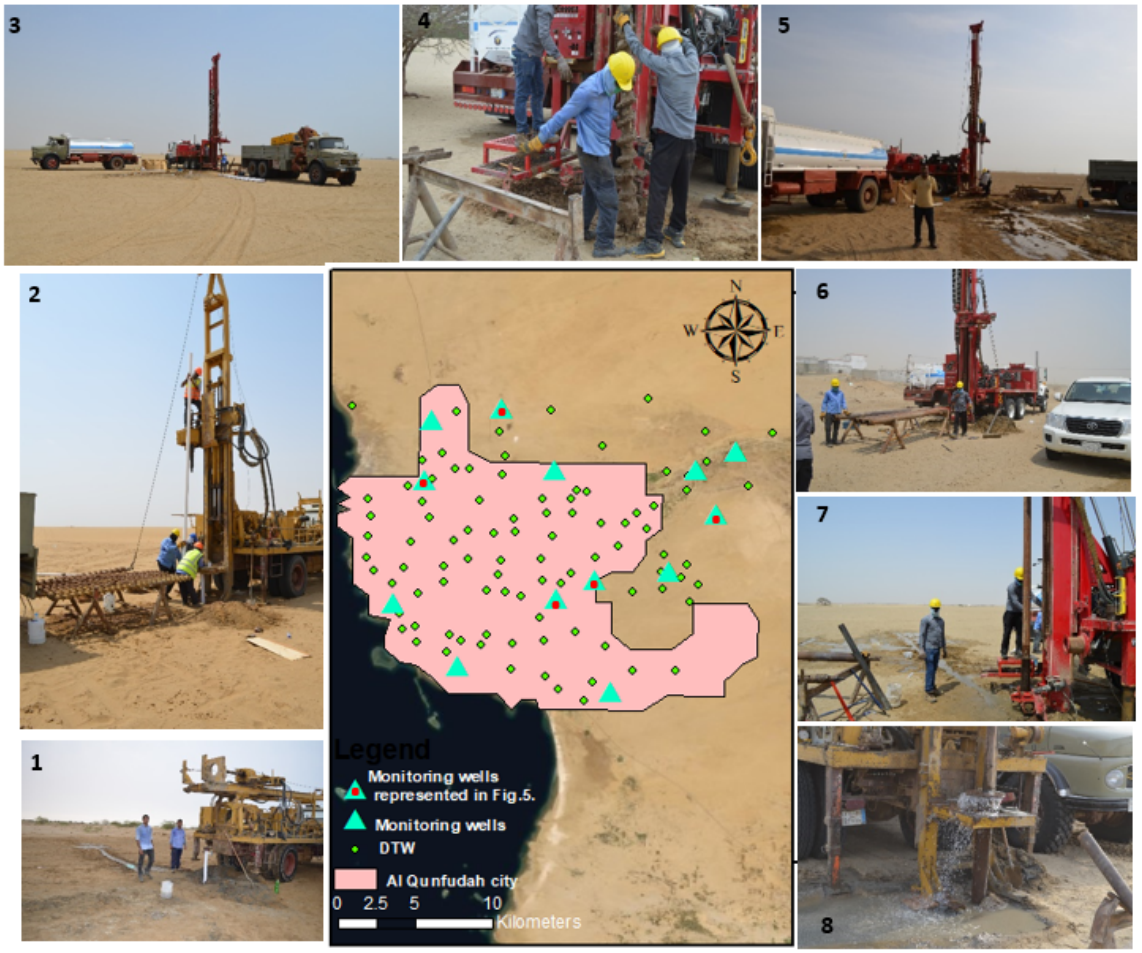

Figure 6. Location map of Al Qunfudah city. Showing the distribution of the drilled wells and field shots for my team members during our field trips (1 to 8) of drilling wells to investigate the depth to water table.

Table 1. Annual Monitoring wells for 13 wells located in the study are, measured for the year of 2017, 2018 and 2019 by the minestry of water and agricultural in Al Qunfuday city.

Well Name	Depth to water in 2017	Depth to water in 2018	Depth to water in 2019
QN-010	15	15	14
Q-15	20	20	19
QM-011	18	16	16
QN-027	17	16	15
QN-010	15	15	14
Q-06	18	17	16
Q-003	17	17	14
QN-009	17	16	15
Q-008	20	20	19
QM-007	20	20	18
Q-01	18	17	16
Q-13	15	15	14
QN-005	18	17	17

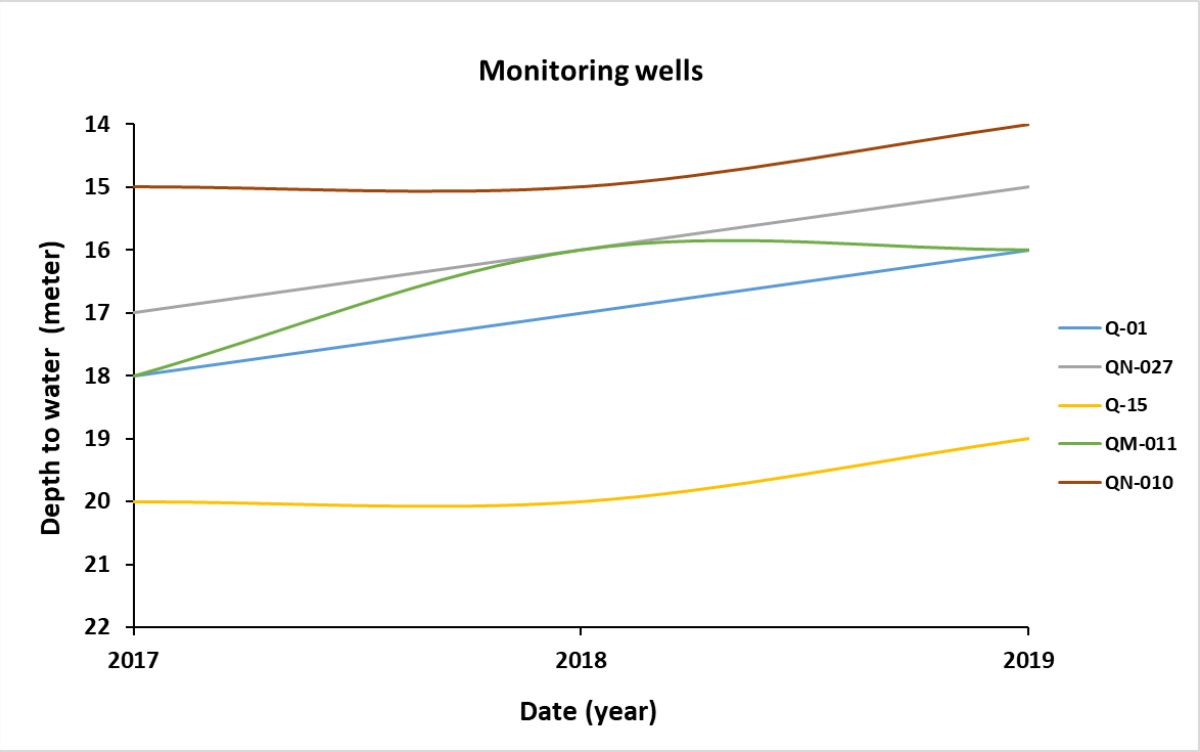

Figure 7. Monitoring wells showing the rise in groundwater levels. The locations of these wells are plotted on (Fig. 1a.)

3.2.2 Downloading and processing of remote sensing datasets

(a) Input remote sensing data: Normalized Difference Vegetation Index

The Normalized Difference Vegetation Index NDVI data product (spatial resolution: 250m) acquired by the National Aeronautics and Space Administration (NASA) MODIS satellite was utilized in this study. The data was downloaded from the NASA's Vegetation Index processing website (https://modis.gsfc.nasa.gov/). The MODIS vegetation index images are produced on 16-days intervals at multiple spatial resolutions; they provide consistent spatial and temporal comparisons of vegetation canopy greenness, leaf area, and chlorophyll and canopy structure. The ArcGIS Marine Geospatial Ecology Tools (MGET, https://mgel.env.duke.edu/mget/) was used to convert HDF format to GeoTiff format. The MODIS NDVI data has been used in a broad range of research activities, such as drought monitoring, global vegetation variation, agricultural and hydrologic modelling (Caccamo et al. 2011; le Maire et al. 2011; Lunetta et al. 2006). In arid and semi-arid areas, climate change and water availability are vital factors affecting vegetation dynamics (Eamus et al. 2006; Naumburg et al. 2005).In arid and semi-arid environments, water table depth is reported to be an important factor affecting the vegetation cover (Jin et al. 2011; Lv et al. 2013). In the shallow, but not in the deep wells, the root zones of vegetation do not reach the water table. Studies have shown that in the arid regions, the root zones of the natural vegetation reach up to the depth of 2 to 7m (Allison and Hughes, 1982; Canadell, 1996; and Nippert and Knapp, 2007).

The DTW and NDVI relationship was investigated; an average NDVI image and a standard deviation image was extracted over each of investigated wells by averaging the NDVI values from images acquired over the period 2015-2018. We averaged multiple NDVI images to capture the vegetative density of each pixel throughout the investigated period instead of using a single NDVI image that may represent spatial vegetation variations relative to a specific season of that year. If the vegetation was supported by shallow groundwater, we expect higher NDVI values and higher variations in NDVI values. These variations are represented by higher standard deviation (STD) values in response to seasonal and inter-annual fluctuations in groundwater levels. Over areas characterized by deep groundwater levels, vegetation will be absent since the roots will not reach the groundwater table and will not be affected by fluctuations in water levels.

(b) Input remote sensing data: Land Surface Temperature (kelvin)

The Land Surface Temperature (LST) (Kelvin) data product 8 daily (spatial resolution: 1000m) acquired by NASA's MODIS Aqua satellite was utilized. The data was downloaded from the LST processing website (https://modis.gsfc.nasa.gov/) that provides an option for periodical data download for specified regions via a free data subscription service. The ArcGIS toolbox Marine Geospatial Ecology Tools (MGET) was used to convert HDF format to geotiff format. LST has been extensively used in multiple research disciplines such as global climate, agriculture, hydrology, ecology

(Carlson, T.N.; Gillies, R.R.; Perry, 1994; Xu, Y.; Shen, 2013), many of which have shown that vegetation intensity is inversely correlated with LST, where vegetation increases with decreasing LST (Deng, et al, 2018). An average LST image and a standard deviation image was extracted over each of investigated wells by averaging the LST values from images acquired over the period 2015-2018. Over areas of shallow groundwater, we expect that the LST values to be low and vary in magnitude (i.e., low standard deviation) in response to seasonal and inter-annual fluctuations in groundwater levels and vice versa over areas with deep groundwater.

(c) Input remote sensing data: Radar backscattering coefficients (dB)

Sentinel-1 is a satellite mission of the European Space Agency (ESA) that uses synthetic aperture radar (SAR) operating in the C-band wavelength region (spatial resolution: 12m). Sentinel-1A radar Ground Range Detected (GRD) scenes were downloaded for ascending acquisition modes from the Sentinel Data (https://asf.alaska.edu). Ascending acquisition modes were selected due to the availability of scenes covering the study area. The following operations were conducted: radiometric calibration and calculation of radar backscatter coefficient (beta naught β0) in decibels (Raney et al., 1994; Small, 2011), speckle and temporal filtering, terrain flattening and geometric correction and co-registration. RBC has been found to be effective in monitoring hydrologic systems including seasonal patterns of flooding (Kasischke et al., 2003; Kim et al., 2014). Average and STD images were generated

from the temporal β0 images acquired over the investigation period (2015-2018). Over areas of shallow groundwater, we expect that the β0 values will be high and vary in magnitude (i.e., high STD) in response to seasonal and inter-annual fluctuations in groundwater levels and vice versa over areas with deep groundwater.

(d) Input remote sensing data: Soil moisture and Ocean Salinity

ESA's Soil Moisture Ocean Salinity (SMOS) Earth Explorer mission is a radio telescope in orbit pointing towards the Earth. The Microwave Imaging Radiometer using Aperture Synthesis (MIRAS) radiometer on this mission picks up faint microwave emissions from Earth's surface to map levels of land soil moisture and ocean salinity. SMOS monthly data (spatial resolution: 0.27° x 0.27°) for ascending acquisitions was downloaded from the Centre Aval de Traitement des Donnees SMOS (CATDS) website (https://www.catds.fr/Products/Available-products-from-CPDC) using FTP File-zilla software. The MGET package was used to extract soil moisture images from the netCDF format, re-project and export the output in GeoTiff format. An average and a STD image was generated from the SMOS images acquired over the investigation period (2015-2018). Over the areas of shallow groundwater, we expect the soil moisture values to be high and vary in magnitude (i.e., high STD) in response to seasonal and inter-annual fluctuations in groundwater levels and vice versa over areas with deep groundwater.

(e) Input remote sensing data: Global Precipitation Measurement

The Global Precipitation Measurement (GPM) mission is a network of satellites which provides global observations on the distribution and intensity of precipitation in the form of rain and snow. The GPM data is helping advance our understanding of Earth's water and energy cycle and is providing accurate and timely information of precipitation to address societal needs (Arthur et al, 2014). Precipitation is the driver of all hydrologic systems; an increase in precipitation increases runoff, surface water levels, groundwater infiltration and storage, and leads to a rise in water table (Gerla, 1992; Vidon, 2001; Park et al, 2008). In this study, GPM (IMERG Final Precipitation L3 Half Hourly (spatial resolution: 0.1° x 0.1°) daily products were downloaded from the Global Precipitation measurement (GPM) website (https://pmm.nasa.gov/data-access/downloads/gpm) using the FTP Filezilla software covering the period of 2015 to 2018. With increased precipitation one should expect shallowing of DTW.

3.3 Development and validation of a conceptual model for shallow groundwater

As described in the previous section, we expect to observe high NDVI, high radar backscatter, high soil moisture, and low LST and relatively large variations in each of these variables (except LST) over areas of shallow groundwater and vice versa over areas characterized by deep groundwater. Following the downloading and processing of the remote sensing products, we tested the merits of our conceptual model by: (1) applying statistical parameters (e.g., mean, maximum, minimum, STD) for all of the digital datasets using cell statistic tools in ArcGIS; and (2) generating time-

enabled mosaic datasets and plotting time series graphs (x-y plots for variables versus time) to examine the temporal change for all variables. Uniformly spaced grid points were used to extract the values from products of different resolutions, and subsequent processing was done on the same grid to achieve computational efficiency. The collected remote sensing products were later checked for consistency and significance.

Six locations were selected: three characterized by shallow groundwater levels (DTW: ≤5 m) and three by deep ground water levels (DTW >5 m) for the purpose of examining whether the areas characterized by shallow groundwater would have a response on one or more of the selected image types (e.g., NDVI, RBC, and LST images, as well as the STD of each of these images) that is different from that over areas of deep groundwater (Figures 5, 6, and 7). The locations for these six wells are shown in Figure 1c. Comparisons of the temporal (2009 to 2018) variations in NDVI values between the three shallow and the three deep groundwater wells are shown in Figure 5, and comparisons for the variations in LST for the same six wells over the same period are shown in Figure 6. The comparisons for the backscatter coefficient variations over a shorter time period (2015 to 2018) are given in Figure 7. The shorter temporal coverage is attributed to the period of operation of the Sentinel-1A mission and scene acquisition dates over the study area (launch date: 2014; first acquisition over study area: 2015).

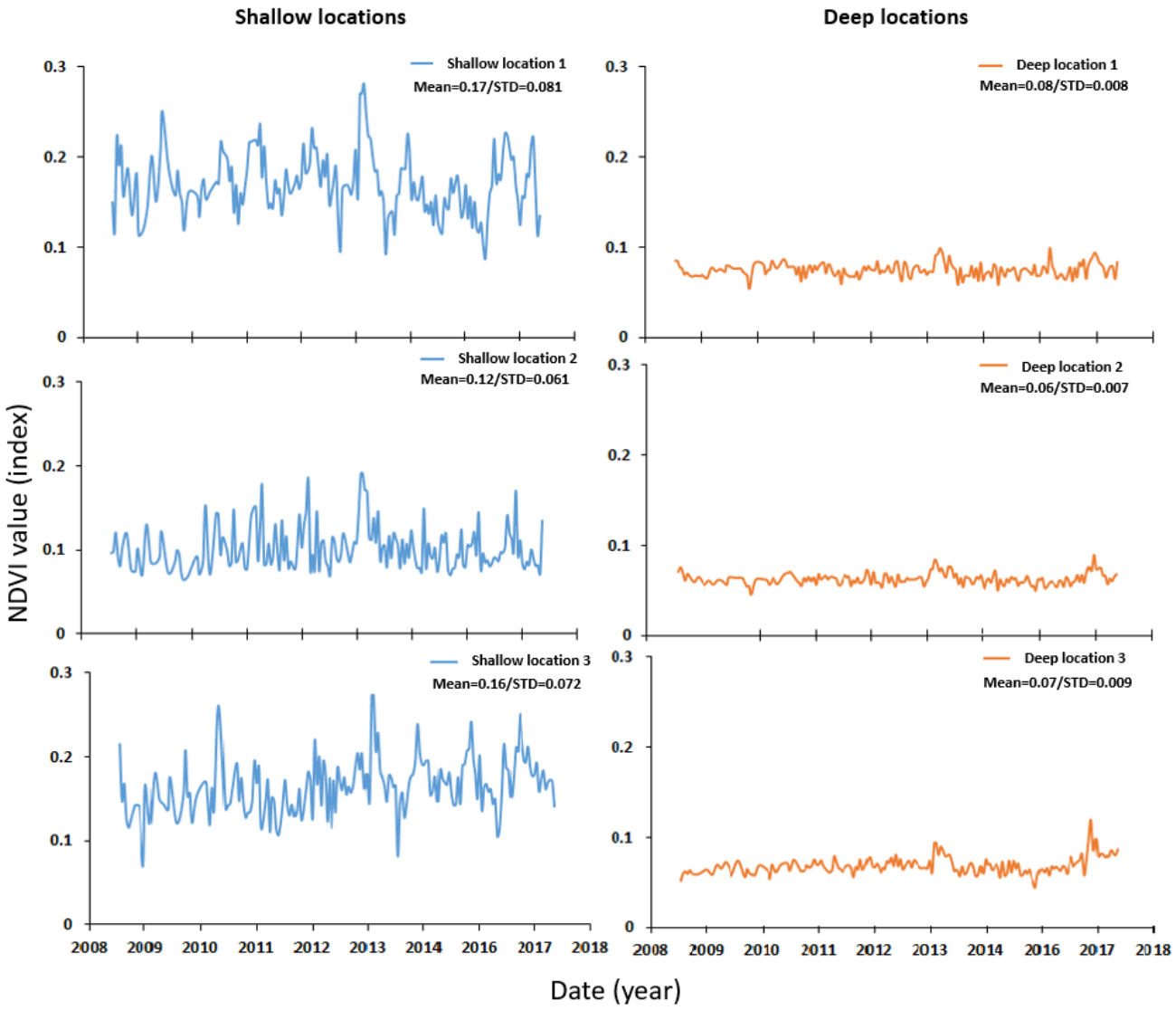

Figure 8. Time series of NDVI. Derived from MODIS 16-daily imagery over three areas characterized by shallow groundwater and three other locations characterized by deep groundwater.

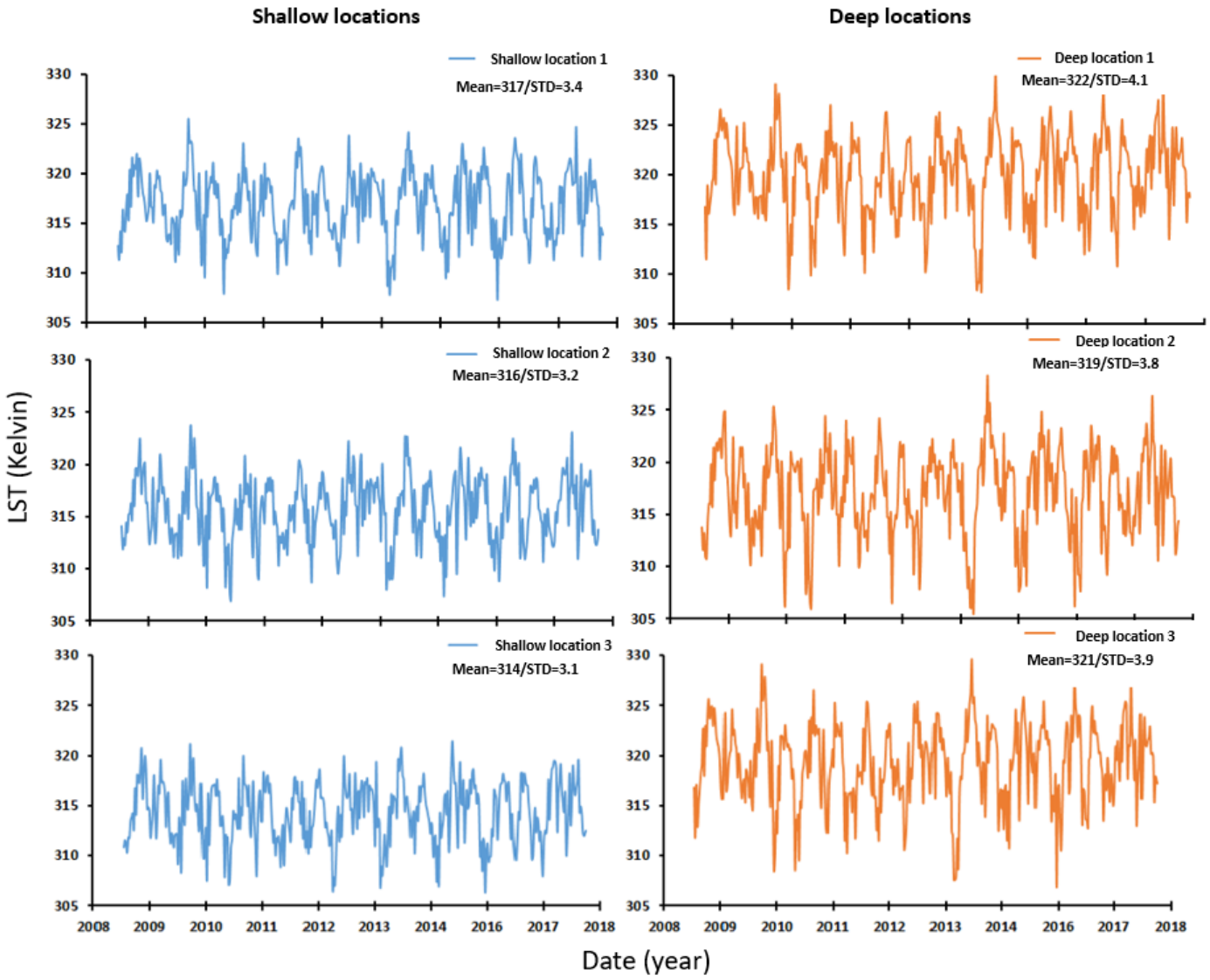

Figure 9. Time series of LST. Derived from MODIS 8-daily imagery over three areas characterized by shallow groundwater and three other locations characterized by deep groundwater.

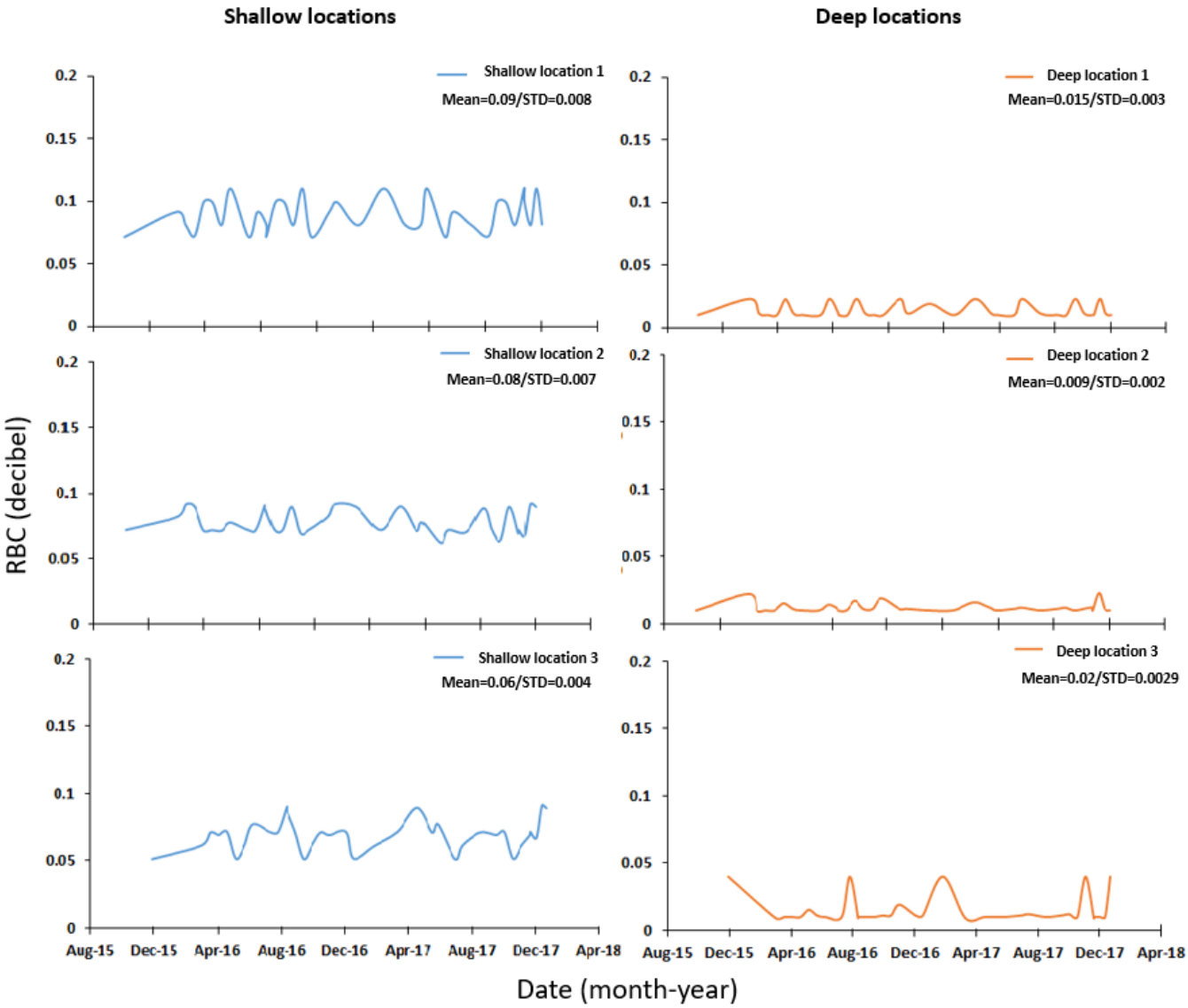

Figure 10. Time series of RBC. In decibel derived from Sentinel-1 over three areas characterized by shallow groundwater and three other locations characterized by deep groundwater.

3.4 Construction and validation of a statistical model to map shallow groundwater occurrences

(a) Screening of the variables

The first step for the construction of the statistical model was to identify the variables to be considered for model development and to determine the optimum combination of significant variables. The screening of variables was conducted using exploratory and stepwise regression. This step gives first-hand insights into the contribution of each variable to the dependent variable (DTW). Only the variables identified as being significant were considered for the statistical model.

We conducted exploratory and stepwise regression and investigated the p-value and R-squared values to determine their significance. We experimented with normalized and non-normalized values to determine which of the two datasets provided the optimum results. During the process, we retained the variables with low p-value and high R-square values; these were considered as being of higher significance and as having a stronger ability to explain the variability of the dependent variable. Following the significance test, the variables were subjected to multicollinearity test using the Variance Inflation Factor (VIF) values (O'Brien, 2007). A variable with VIF higher than 7.5 was considered redundant with the second highest VIF and was omitted. This step was performed for all the redundant variables by dropping one variable at a time without reducing the overall performance of the model. The redundancy test was conducted iteratively to ensure that significant and non-redundant variables were not

eliminated. Our goal of this exercise was to obtain the highest overall R-squared value with a minimal number of significant variables. Only six variables (GPM, LST, NDVI, RBC, STD of LST and STD of NDVI) were shortlisted for further consideration as shown in Figure 9. The relative significance of each of the short-listed variables was accomplished using the normalized data set.

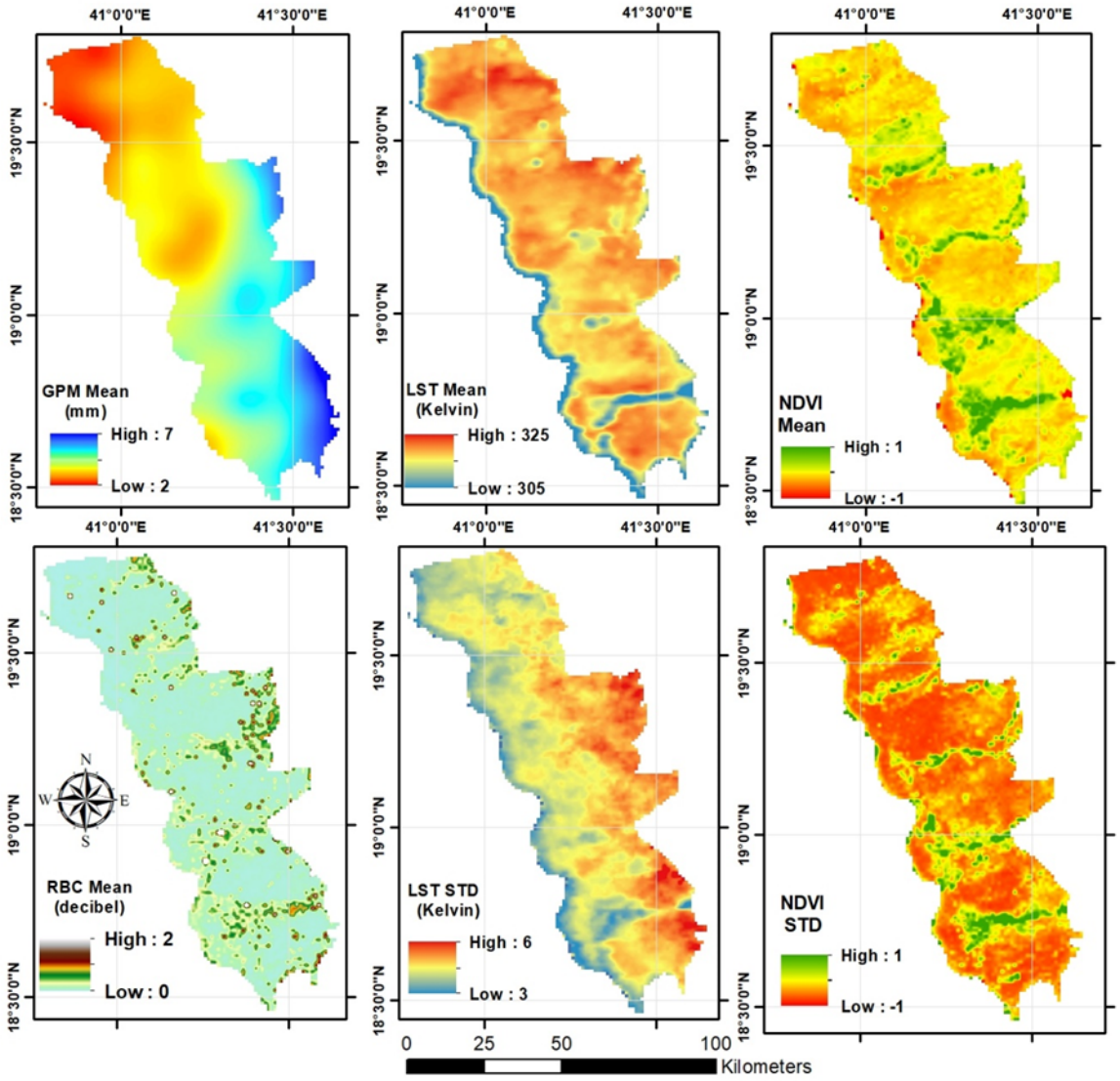

Figure 11.The significant satellite-based variables. Include mean precipitation (from GPM), the mean and standard deviation values of LST and NDVI (both from MODIS), and RBC (from Sentinel-1A), all of which were extracted throughout the study period (2015 to 2018).

(b) Identification of the optimum model

Two statistical approaches, the Multivariate Linear Regression (MR) and Artificial Neural Networks (ANN), were adopted to model the relationships between the shortlisted input variables (NDVI, LST, RBC, GPM, STD of NDVI, and STD of LST) and depth to water table (response variable. The training subset comprised 80% of the data points and was used to construct the model, whereas the remaining 20% were used to evaluate the performance of the models and were not used for model development. The same sets (training and testing datasets) were used for model development and validation of the MR and ANN models.

(c) Multivariate linear regression

The MR method describes a multivariate linear relationship between one or more predictor variables and a response variable (Sahour, 2020). The model assumes that the magnitude of the dependent variable is represented by the sum total of all the contributions of the individual variables; any unexplained contribution is represented by a model bias or a constant. The regression line for n independent variables X1, X2, X3 ...., Xn can be expressed as follows:

$$Y = (B_0) + (B_1 * X_1) \pm (B_2 * X_2) \pm \ldots\ldots \pm (B_n X_n),$$

Where Y is the predicted value of the target variable, B_0 is the model bias and B_1 through B_n are individual model coefficients. Spatial Statistics extension in ArcGIS was used in this analysis.

(d) ANN model

ANN utilizes algorithms to model the complex and non-linear relationships (Karlaftis and lahogianni, 2011; Huang 2009) among various factors controlling the response variable, in our case the DTW. The ANN is based on connection of neurons, a process that is designed to replicate the functions of neurons in the nervous systems of organisms; they pass information between one another, a structure that enables ANNs to be trained and to learn complex interactions. A fitting neural-network module of MATLAB R2019 was utilized to detect shallow groundwater.

A simplified flowchart of our constructed ANN model is provided in Figure 10. The hyperparameter that controls the model structure (e.g., number of layers, number of hidden neurons, and number of epochs) was set before the learning process was conducted. An error technique was applied to determine the optimal number of hyperparameters; this was accomplished by gradually adding the number until the predicted and observed values begin to mimic each other. The model performance was evaluated using the mean squared normalized error (MSE) performance function. The widely used backpropagation learning algorithm (Huang, 2009) in a fitting neural-network modeling was applied and the number of hidden neurons was increased until the model performance plateaued at 16 neurons.

3.5. Selection of the optimum model to map shallow groundwater across Al Qunfudah Province

Following the development of the MR and ANN models, their performance was assessed and the model with the highest performance was used to map the distribution of shallow groundwater throughout the Al-Qunfudah Province.

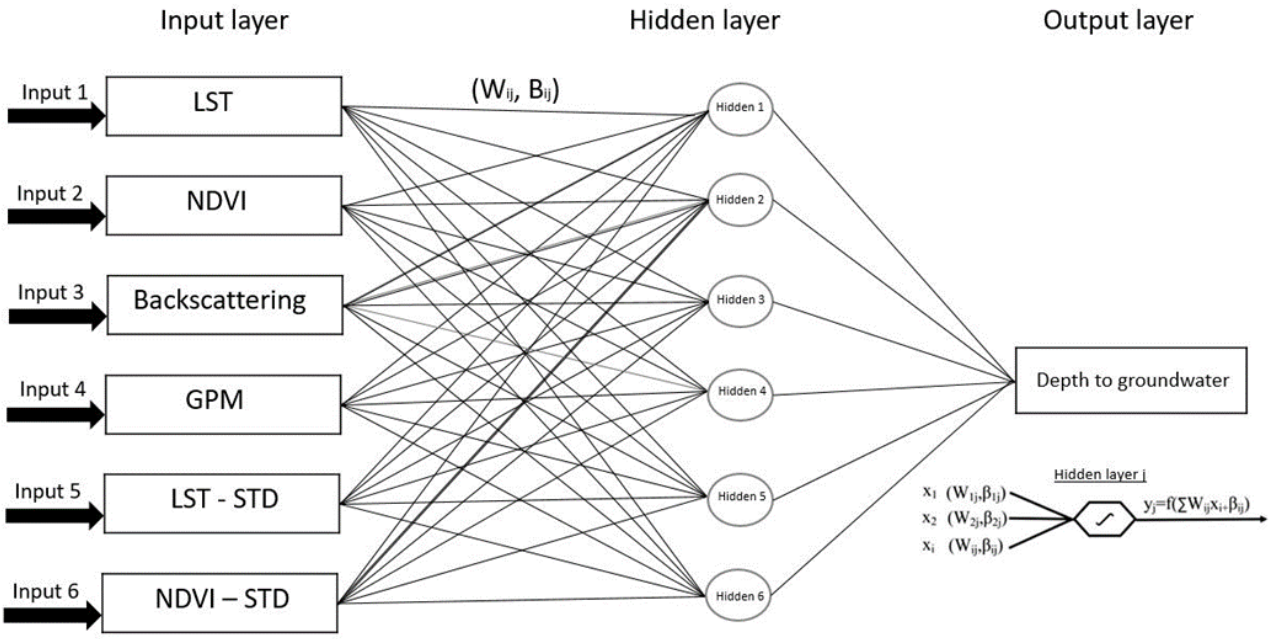

Figure 12. Schematic diagram for the constructed Fitting ANN. Wij represents the weight term and the βij the bias term; these terms were assigned between the input layer i and the hidden layer j during the learning procedure; f is the transfer function, xi the input from input layer i, and yj the output related to the hidden layer j.

CHAPTER 4

RESULTS AND DISCUSSION

4.1 Results

Findings from the exploratory and stepwise regression investigations revealed that SMOS was redundant with RBC possibly because radar backscatter is controlled, at least in part, by SMOS (Karki et al, 2019). SMOS data sets were removed from further consideration and RBC was preferred over SMOS because of its higher spatial resolution. The STD of RBC was found to be less significant than the remaining variables and was dropped as well. The elimination of SMOS and STD of RBC did not affect the overall performance of the model. Out of 8 variables under initial consideration, only 6 variables (LST, NDVI, RBC, GPM, STD of LST, and STD of NDVI) were shortlisted for model construction (Fig.8). The relative significance of each of the short-listed variable set is given (in percentage) in Table 1. LST was found to be the most significant variable (43.2%), whereas each of the remaining 5 variables accounted for 9 to 15% of the observed variations in the response variable.

Each of the determining variables exhibited a unique response to the DTW as shown in Table 2. The table lists the MR coefficients for each variable in predicting DTW. The sign (±) in front of the coefficient for each selected variable indicates the nature (positive/negative) of the relationship between the variable in

question and the response. As expected, in areas experiencing shallow groundwater, soil moisture increases causing an increase in RBC and a decrease in LST and in its variability (STD of LST). One would also expect an increase in NDVI and in its standard deviation in areas characterized by shallow groundwater. This is true for the standard deviation of NDVI, but not for the mean of NDVI. One possible explanation for this discrepancy is the assumption that all the observed temporal and spatial variations in NDVI are caused by variations in the intensity of natural vegetation. While this assumption is true over much of the desert landscape, it does not necessarily apply over farmed areas where groundwater could be extracted from deep or shallow depths. Also, the vegetative cover over the desert landscape could remain dormant and dry for long periods, until one or more of the infrequent, but extensive precipitation events occur and cause the desert to green. Over these irrigated areas and during these sporadic precipitation events, the NDVI values could be high, yet the DTW is not necessarily shallow. As expected, the MR and ANN yielded different levels of accuracies (Table 3) due to the inherent differences in these models (linear versus complex relationships).

Table 2. Selected variables and their relative significance (in percentage) from the MR model.

	Variables	Relative Significant
1	LST (mean)	43.2%
2	NDVI (mean)	15.4%
3	NDVI (STD)	11.0%
4	LST (STD)	10.8%
5	RBC (mean)	10.2%
6	GPM	9.4%

Table 3. Multivariate regression coefficients for each of the selected variables.

	Variables	Coefficients
1	LST (mean)	2.30
2	NDVI (mean)	42.99
3	NDVI (STD)	-53.86
4	LST (STD)	4.19
5	RBC (mean)	-3.25
6	GPM	-2.02

As expected, the MR and ANN yielded different levels of accuracies (Table 3) due to the inherent differences in these models (linear versus complex relationships). Both models yielded high accuracy in predicting the target with a slight enhancement of the ANN (accuracy: 92%) over the MR model (accuracy: 88%). The prediction accuracy was based on the ability of the model to predict shallow (≤5 m) and deep groundwater (>5 m); six variables (LST, NDVI, RBC, GPM, STD of LST, STD of NDVI) were used by both models for prediction purposes. In both cases, inclusion of additional variables did not improve the model accuracy. We used the optimum model (ANN model) that was developed over Al Qunfudah city and surroundings (area: 294 km2) to map shallow groundwater across the entire Al Qunfudah Province (area: 4680 km2; Fig.10). The generated ANN model output (derived matrix) was utilized in an ArcGIS 10.6 platform for mapping the distribution of the shallow groundwater occurrences across the province.

Table 4. ANN and MR models accuracies in predicting the testing data. The numbers in bold indicate correct prediction for each model.

	Testing Datasets	**well predicted**	**Not Predicted**	**Accuracy**
Artificial Neural Network	25	23	2	92%
Multivariate Regression	25	22	3	88%

ANN predicted details	Predicted shallow location	Predicted deep location	**MR predicted details**	Predicted shallow location	Predicted deep location
Shallow location	**6**	2	Shallow location	**5**	3
Deep location	0	**17**	Deep location	0	**17**

4.2 Discussion

The prediction of depth to groundwater in our study area involves developing an understanding of the variables indicative of the presence of shallow groundwater and the complex interactions among these variables. A conceptual model was first developed that predicts areas with shallow groundwater indicated by high NDVI (mean and STD), RBC (mean and STD) and low LST (mean and STD) values compared to areas with deep groundwater. This model was tested visually over 13 locations and was then validated and refined using an exploratory stepwise regression analysis. Six of the eight variables were selected and two were omitted given their lower significance and/or redundancy. An MR model was developed to determine the level of variance each variable explains in the response variable and the nature of the relationship between shallow groundwater occurrences and the individual variables.

The MR model was used to determine the comparative significance of each variable towards the DTW. Although simplistic, this information provided first-hand insights into the contribution of each variable. These estimated contributions represent the minimum contribution of each variable and do not reflect the complex interaction among variables which could be significant in natural environments. Inspection of Table 1 reveals that the most significant (43.2%) variable is the LST (mean), whereas the remaining five variables have sub-equal significance (range: 9.2% to 15.4%). These include NDVI (mean and STD), RBC (mean), and Precipitation. Although SMOS data sets appeared to be

significant, it was redundant with RBC, and thus it was dropped. Similarly, the standard deviation of the RBC was dropped from the model because it did not enhance the model performance. This may be because radar backscatter is already explaining the variance present in dependent variable.

The MR model was used to infer the nature of relationship between the independent variable and the DTW. The information provided in Tables 2 can be used to interpret the nature of the relationship between the DTW and the individual variables. In simple terms, the mathematical sign (±) associated with each coefficient provides the information about the type of the response it offers to DTW. For example, areas of shallow groundwater (low DTW) are characterized by relatively low LST (mean, STD), high RBC (mean), high variation in NDVI (STD), and high precipitation compared to areas characterized by deep groundwater (high DTW). With the exception of the NDVI (mean), these observations are consistent with our conceptual model and with the visual inspection of the temporal variations over the 13 test wells (Figures 1c. and 4). The NDVI (mean) is showing a decrease in NDVI value in areas of shallow groundwater and vice versa for deep groundwater. This discrepancy is probably related to the fact that our procedure was not designed to differentiate between natural vegetation and irrigated farmlands. The former is indicative of shallow groundwater, whereas the latter does not necessarily indicate the presence of shallow groundwater in semi-desert environments.

The ANN provided enhanced prediction over the MR model (Table 3) and thus, it was selected for mapping the distribution of shallow groundwater across Al Qunfudah Province. This is to be expected given that the ANN models can account for the variations in data distributions and patterns, and can even consider the smallest and less obvious fluctuations in data sets (Haykin, 1994; Govindaraju at el, 2010).

To better understand the distribution of the shallow and deep groundwater across the study area, and their controlling factors, we created 3D renderings of the generated DTW (Fig.10a) and AAP (Fig.10b) each draped over the digital elevation model (DEM) that was extracted from the Advanced Spaceborne Thermal Emission and Reflection Radiometer (ASTER) image. Additional 3D renderings were generated for a slope image DEM (Fig.11a) and a natural color composite (Esri Digital Globe, 2019) map (Fig. 11b) each draped over the DEM. Inspection of Figures 10 and 11 reveal some general features. Shallow groundwater along the coastal plain in areas proximal to the coastline (width: 3 to 5 km) and within the main valleys that collect runoff from precipitation over the Red Sea Hills. The most prominent of these main valleys is E-W trending Wadi Hali. The Wadi Hali catchment receives higher precipitation (AAP: 192 mm/yr.) than those to the north (AAP: 152 mm/yr.) (Fig.10b). This could explain why Wadi Hali, but not wadis Ganunah, Al ahsabah has shallow groundwater. Not only do the southern highlands receive higher precipitation, but also the

general slope of their coastal plain is gentle (slope: 0 to 3°; average slope: 2.5°) comparted to the northern coastal plain areas (slope: 3 to > 6°; average slope: 6°; Fig.11a). The steeper the slope, the less the infiltration and the deeper the groundwater.

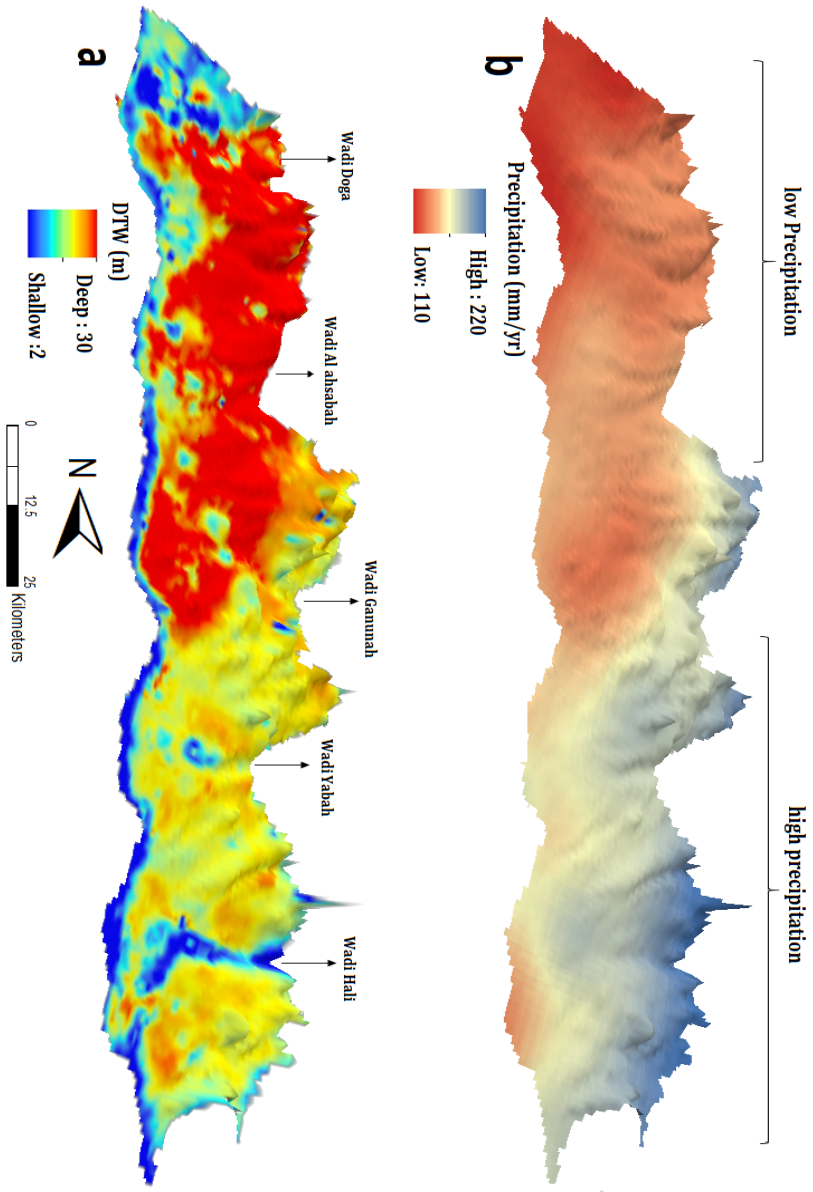

Figure 13. (a) 3D rendering of the ANN-generated DTW map for Al Qunfudah Province. Draped over the DEM (vertical exaggeration: 30), (b) Average annual precipitation (2014 to 2018) draped over DEM for the Al Qunfudah Province.

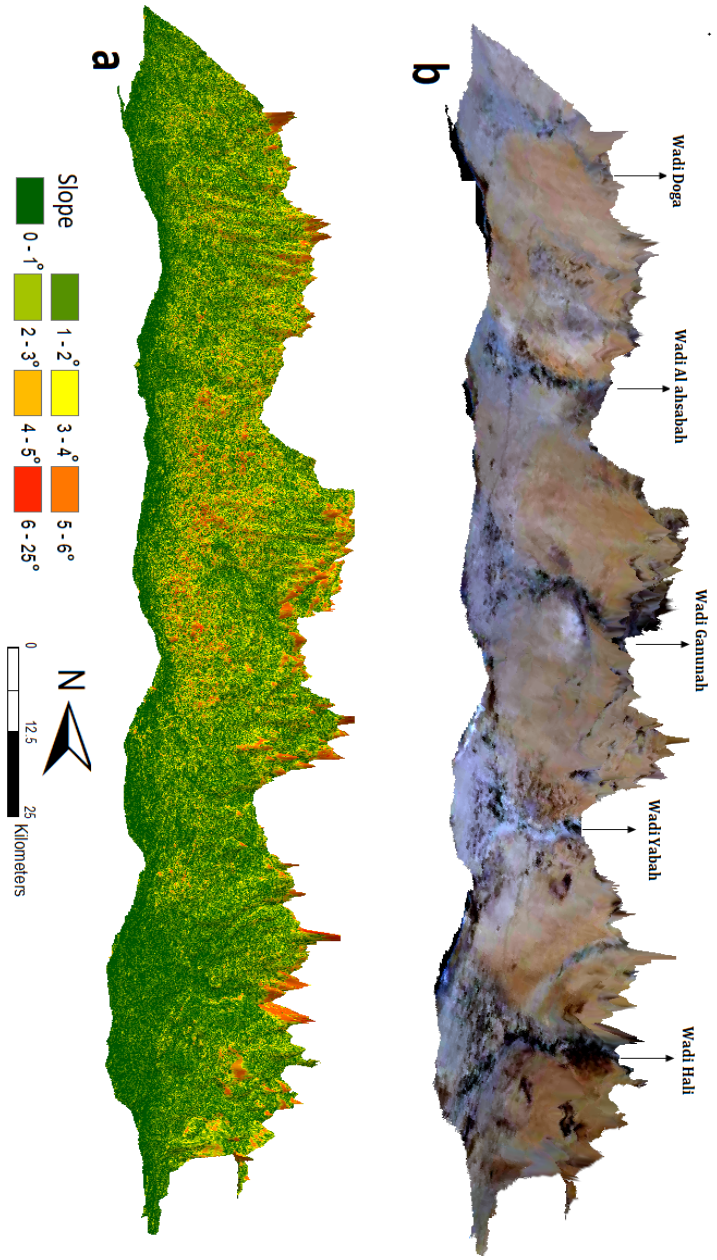

Figure 14. (a) 3D rendering of slope map for Al Qunfudah Province. Draped over DEM (vertical exaggeration: 30), (b) a natural color composite map generated from Esri Digital Globe draped over DEM for the Al Qunfudah Province.

We showed that the spatial variations in precipitation could explain at least in part the modeled variations in the DTW across Al Qunfudah Province, but it does not explain the observed rise in groundwater levels (Fig.4). Inspection of Table 4 shows that there has been an increase in the AAP over Al Qunfudah Province over the past three years (2017–2019: 162 mm/yr) compared to the preceding three years (2014–2016: 139 mm/yr). The table also shows that there has been a similar increase in the AAP over the watersheds draining into Al-Qunfudah Province. In the years 2017–2019, the AAP was high (Hali watershed: 192 mm; Yabah: 170 mm; Ganunah: 163 mm, Al ahsabah: 158 mm; Doga: 152 mm) compared to the preceding three years (Hali: 171 mm; Yabah: 151 mm; Ganunah: 140 mm; Al ahsabah: 141 mm; and Doga: 127 mm). The increase in precipitation over Al-Qunfudah Province and over the watersheds that drain into the Province will lead to increased infiltration and recharge of the alluvial aquifers underlying the Al-Qunfudah coastal plain causing a rise in groundwater levels in these aquifers. Thus, the observed increase in groundwater levels over the past three years (Fig.4) is likely to be related to increased precipitation.

Table 5. AAP over Al Qunfudah Province and the watersheds feeding it during recent years (2017-2019) compared to the preceding three years (2014-2016).

	AAP (2014-2016) mm	**AAP (2017-2019) mm**
Doga watershed	127	152
Al ahsabah watershed	141	158
Ganunah watershed	140	163
Yabah watershed	151	170
Hali watershed	171	192
Al Qunfudah Province	139	162

4.2 Limitations

There are several limitations with the applied methodology. The developed models were developed for the coastal plain of the Al Qunfudah Province. Thus, it probably could potentially be applied to similar settings along the Red Sea Hills or elsewhere, but not to areas with different geologic and hydrologic settings (e.g., mountainous terrains). The number of training data was limited in our models. Like any other machine learning models, addition of more training data will significantly improve the predictability. Several of our remote sensing datasets data sets (e.g. RBC, DEM) are available at high-resolution (12 to 30 m), whereas others (e.g., GPM; resolution: 0.1° x 0.1°) are very coarse. In other words, we had to combine high-resolution with low-resolution datasets, a process that reduces the accuracy of our statistical model predictions. During this exercise, the predictability of the model can be improved by providing the higher spatial resolution products especially for precipitation.

CHAPTER 5

SUMMARY AND CONCLUSION

In this study, we developed and successfully applied methodologies that rely heavily on readily available temporal, visible and near-infrared (VNIR), radar, and thermal remote sensing data sets and field data, and statistical approaches to map the distribution of shallow groundwater occurrences in Al Qunfudah Province (Saudi Arabia) and to identify the factors controlling their development.

The study focused on developing statistical models to identify shallow groundwater occurrences over large areas using readily available remote sensing datasets. We used the coastal zone of Al Qunfudah Province, southwest Saudi Arabia as a test site. A conceptual model was developed over the Qunfudah city and its surroundings, where field data is available. The model predicts that areas characterized by shallow groundwater could have high NDVI (mean, STD), high RBS (mean, STD), and low LST (mean, STD) compared to areas with deep groundwater levels.

A comprehensive spatio-temporal database was constructed, and the conceptual model was validated visually using field data (water levels in 13 wells) and remote sensing data over these wells.

We constructed an ANN and MR models to map the distribution of shallow groundwater occurrences in the AL-Qunfudah city and surroundings, tested the statistical models against field data, and selected the optimum model (ANN) to map the DTW across the entire Al-Qunfudah Province. The statistical models were constructed using a randomly selected training data sets (80% of the total), whereas the remaining data sets (20%) were used for testing purposes. Our findings indicated an enhanced performance for the ANN model (92%) over the MR (88%) in predicting the distribution of shallow groundwater.

Temporal correlations of the groundwater levels and satellite-based precipitation suggest that there has been an increase in the AAP over Al Qunfudah Province over the past three years (2017-2019: 162 mm/yr) compared to the preceding three years (2014-2016: 139 mm/yr).

Even though this project focuses on Al Qunfudah Province and its surrounding, the adopted approach can potentially be replicated over many parts of the arid world with similar climatic, geologic, and hydrologic setting. The applications of such technologies are cost-effective and could have significant societal benefits. These include, but are not limited to, locating additional fresh water supplies over extensive arid areas worldwide and addressing environmental

problems arising from rise in groundwater levels that may cause health problems to populations and properties (e.g., foundations, structures, etc.).

REFERENCES

Abdullah, R. (2014). Integrated Pollutant Fingerprinting of Shallow Groundwater using Resistivity Imaging Profiling and Hydrochemical Methods at the Beriah Landfill Site. International Journal of Applied Environmental Sciences, 9(4), 2161-2173.

Abotalib, A. Z., Sultan, M., & Elkadiri, R. (2016). Groundwater processes in Saharan Africa: implications for landscape evolution in arid environments. Earth-Science Reviews, 156, 108-136.

Abu, Rizaiza. ; Hasan. (1989). Water requirements versus water availability in Saudi Arabia. Journal of Water Resources Planning and Management. vol. 115, 64–74, 1989.

Allison, G. B., & Hughes, M. W. (1983). The use of natural tracers as indicators of soil-water movement in a temperate semi-arid region. Journal of Hydrology, 60(1-4), 157-173.

Al-Sefry, S. A., & Şen, Z. (2006). Groundwater rise problem and risk evaluation in major cities of arid lands–Jedddah Case in Kingdom of Saudi Arabia. Water Resources Management, 20(1), 91-108.

Anderson, J. K., Wondzell, S. M., Gooseff, M. N., & Haggerty, R. (2005). Patterns in stream longitudinal profiles and implications for hyporheic exchange flow at the HJ Andrews Experimental Forest, Oregon, USA. Hydrological Processes: An International Journal, 19(15), 2931-2949.

Bayumi, T. H., Alyamani, M. S., Subyani, M. S., & Al-Ahmadi, M. E. (2000). Analytical study of flood problems and groundwater rise in the Jeddah District. Final Report of Project, 606, 418.

Bob, M., Rahman, N., Elamin, A., & Taher, S. (2016). Rising groundwater levels problem in urban areas: a case study from the Central Area of Madinah City, Saudi Arabia. Arabian Journal for Science and Engineering, 41(4), 1461-1472.

Caccamo, G., Chisholm, L. A., Bradstock, R. A., & Puotinen, M. L. (2011 Assessing the sensitivity of MODIS to monitor drought in high biomass ecosystems. Remote Sensing of Environment, 115(10), 2626-2639.

Canadell, J., Jackson, R. B., Ehleringer, J. B., Mooney, H. A., Sala, O. E., & Schulze, E. D. (1996). Maximum rooting depth of vegetation types at the global scale. Oecologia, 108(4), 583-595.

Carlson, T.N.; Gillies, R.R.; Perry, E.M. (1994) A method to make use of thermal infrared temperature and NDVI measurements to infer surface soil water content and fractional vegetation cover. Remote sensing reviews. 19, 161–73.

Deng, Y., Wang, S., Bai, X., Tian, Y., Wu, L., Xiao, J.,& Qian, Q. (2018). Relationship among land surface temperature and LUCC, NDVI in typical karst area. Scientific reports, 8(1), 1-12.

Donohue, R. J., McVICAR, T. R., & Roderick, M. L. (2009). Climate-related trends in Australian vegetation cover as inferred from satellite observations, 1981–2006. Global Change Biology, 15(4), 1025-1039.

Eamus, D., Froend, R., Loomes, R., Hose, G., & Murray, B. (2006). A functional methodology for determining the groundwater regime needed to maintain the health of groundwater-dependent vegetation. Australian Journal of Botany, 54(2), 97-114.

Essam, D., Ahmed, M., Abouelmagd, A., & Soliman, F. (2020). Monitoring temporal variations in groundwater levels in urban areas using ground-penetrating radar. Science of The Total Environment, 703, 134986.

Gleick, P. H., Pacific Institute for Studies in Development, Environment, and Security & Stockholm Environment Institute. Water in crisis: A guide to the world's fresh water resources. New York, 1993, Oxford Univ Press. 473p.1993–9.

Gerla, P. J. (1992). The relationship of water-table changes to the capillary fringe, evapotranspiration, and precipitation in intermittent wetlands. Wetlands, 12(2), 91-98.

Haykin, S. (1994). Neural networks: a comprehensive foundation. Prentice Hall PTR.

Hoffmann, J. (2005). The future of satellite remote sensing in hydrogeology. Hydrogeology Journal, 13(1), 247-250.

Hou, A.Y.; Kakar, R.K.; Neeck, S.; Azarbarzin, A.A.; Kummerow ,C.D.; Kojima, M.; Oki R.; Nakamura, K.; Iguchi, T. (2014). The global precipitation measurement mission. Bulletin of the American Meteorological Society. 95,701–22.

Hötzl, H., & Zötl, J. G. (1978). Climatic changes during the Quaternary period. In Quaternary Period in Saudi Arabia (pp. 301-311). Springer, Vienna.

Huang, Y. (2009). Advances in artificial neural networks–methodological development and application. Algorithms, 2(3), 973-1007.

Huang, F., Zhang, D., & Chen, X. (2019). Vegetation Response to Groundwater Variation in Arid Environments: Visualization of ResearchEvolution, Synthesis of Response Types, and Estimation of Groundwater Threshold. International journal of environmental research and public health, 16(10), 1849.

Jado A.; Zo tl J. (1984). Quaternary period in Saudi Arabia, vol 2: sedimentological, hydrogeological, hydrochemical, geomorphological, and climatological investigations in western Saudi Arabia. Wien, New York.

Jin, X. M., Schaepman, M. E., Clevers, J. G., Su, Z. B., & Hu, G. C. (2011). Groundwater depth and vegetation in the Ejina area, China. Arid land research and management, 25(2), 194-199.

Karlaftis, M. G., & Vlahogianni, E. I. (2011). Statistical methods versus neural networks in transportation research: Differences, similarities and some insights. Transportation Research Part C: Emerging Technologies, 19(3), 387-399.

Karki, S., Sultan, M., Alsefry, S., Alharbi, H., Emil, M. K., Elkadiri, R., & Alfadail, E. A. (2019). A remote-sensing-based intensity–duration threshold, Faifa Mountains, Saudi Arabia. Natural Hazards & Earth System Sciences, 19(6).

Kasischke, E. S., Smith, K. B., Bourgeau-Chavez, L. L., Romanowicz, E. A., Brunzell, S., & Richardson, C. J. (2003). Effects of seasonal hydrologic patterns in south Florida wetlands on radar backscatter measured from ERS-2 SAR imagery. Remote sensing of environment, 88(4), 423-441.

Kim, J. W., Lu, Z., Jones, J. W., Shum, C. K., Lee, H., & Jia, Y. (2014). Monitoring Everglades freshwater marsh water level using L-band synthetic aperture radar backscatter. Remote sensing of environment, 150, 66-81.

Lunetta, R. S., Knight, J. F., Ediriwickrema, J., Lyon, J. G., & Worthy, L. D. (2006). Land-cover change detection using multi-temporal MODIS NDVI data. Remote sensing of environment, 105(2), 142-154.

Lv, J. J., Wang, X. S., Zhou, Y. X., Qian, K. Z., Li, W., Eamus, D., & Tao, Z. P. (2012). Groundwater-dependent distribution of vegetation in Hailiutu River catchment, a semi-arid region in China. Ecohydrology 6 (1): 142–149.

Mohamed, A., Sultan, M., Ahmed, M., Yan, E., & Ahmed, E. (2016). Aquifer recharge, depletion, and connectivity: Inferences from GRACE, land surface models, geochemical, and geophysical data. GSA Bull.

Motagh, M., Djamour, Y., Walter, T. R., Wetzel, H. U., Zschau, J., & Arabi, S. (2007). Land subsidence in Mashhad Valley, northeast Iran: results from InSAR, levelling and GPS. Geophysical Journal International, 168(2), 518-526.

Naumburg, E., Mata-Gonzalez, R., Hunter, R. G., Mclendon, T., & Martin, D. W. (2005). Phreatophytic vegetation and groundwater fluctuations: a review of current research and application of ecosystem response modeling with an emphasis on Great Basin vegetation. Environmental Management, 35(6), 726-740.

Nippert, J. B., & Knapp, A. K. (2007). Linking water uptake with rooting patterns in grassland species. Oecologia, 153(2), 261-272.

O'brien, R. M. (2007). Quality & Quantity. A caution regarding rules of thumb for variance inflation factors, 41(5), 673-690.

Omolaiye, G. E., Aayolabi, E., Ololade, I., & Unuevho, C. (2011). Mapping the depth to groundwater using ground penetrating radar (gpr) in an oil producing community of western niger delta. Journal of Environmental Hydrology, 19

Pfister, L., McDonnell, J. J., Hissler, C., & Hoffmann, L. (2010). Ground-based thermal imagery as a simple, practical tool for mapping saturated area connectivity and dynamics. Hydrological Processes, 24(21), 3123-3132.

Raney, R. K., Freeman, T., Hawkins, R. W., & Bamler, R. (1994, August). A plea for radar brightness. In Proceedings of IGARSS'94-1994 IEEE International Geoscience and Remote Sensing Symposium (Vol. 2, pp. 1090-1092). IEEE.

R. S. (2010). Govindaraju and A. R. Rao, Artificial Neural Networks in Hydrology. New York, NY, USA: Springer.

Sahour, H.; Sultan, M.; Vazifedan, M.; Abdelmohsen, K.; Karki, S.; Yellich, J.A.; Gebremichael, E.; Alshehri, F.; Elbayoumi, T.M. Statistical Applications to Downscale GRACE-Derived Terrestrial Water Storage Data and to Fill Temporal Gaps. Remote Sens.2020, 12, 533.

Salama, R. B., Tapley, I., Ishii, T., & Hawkes, G. (1994). Identification of areas of recharge and discharge using Landsat-TM satellite imagery and aerial photography mapping techniques. Journal of hydrology, 162(1-2), 119-141.

Schuetz, T.; Weiler, M.(2011). Quantification of localized groundwater inflow into streams using ground-based infrared thermography. Geophys Res Lett. 383.

Sources: Esri, DigitalGlobe.(2019) GeoEye, i-cubed, USDA FSA, USGS, AEX, Getmapping, Aerogrid, IGN, IGP, swisstopo, and the GIS User Community.

Stern, R. J., & Kröner, A. (1993). Late Precambrian crustal evolution in NE Sudan: isotopic and geochronologic constraints. The Journal of Geology, 101(5), 555-574.

Sultan, M.; Ahmed, M.; Wahr, J.; Yan, E.; Emil, M. K. Monitoring aquifer depletion from space: case studies from the Saharan and Arabian aquifers. Remote sensing of the terrestrial water cycle. Wiley, Hoboken.2014, pp 347–366.

Sultan, M.; Chamberlain, K.R.; Bowring, S.A.; Arvidson, R.E.; Abuzied, H.; El Kaliouby, B. (1990). Geochronologic and isotopic evidence for involvement of pre-Pan-African crust in the Nubian Shield, Egypt.Geology.188,761–4.

Sultan, M., Wagdy, A., Manocha, N., Sauck, W., Gelil, K. A., Youssef, A. F.& Jones, C. (2008). An integrated approach for identifying aquifers in transcurrent fault systems: The Najd shear system of the Arabian Nubian shield. Journal of Hydrology, 349(3-4), 475-488.

Sulaiman, A., Elawadi, E., & Mogren, S. (2018). Gravity interpretation to image the geologic structures of the coastal zone in al Qunfudhah area, southwest Saudi Arabia. Geophysical Journal International, 214(3) , 1623-1632.

Small, D. (2011). Flattening gamma: Radiometric terrain correction for SAR imagery. IEEE Transactions on Geoscience and Remote Sensing, 49(8), 3081-3093.

Tweed, S. O., Leblanc, M., Webb, J. A., & Lubczynski, M. W. (2007). Remote sensing and GIS for mapping groundwater recharge and discharge areas in salinity prone catchments, southeastern Australia. Hydrogeology Journal, 15(1), 75-96

Taylor, R.G.; Scanlon, B.; Döll, P.; Rodell, M.; Van, Beek R.; Wada, Y.; Longuevergne, L.; Leblanc M.; Famiglietti, J.S.; Edmunds, M.; Konikow, L.(2013). Ground water and climate change. Nat Clim Chang., 3: 322–329.

Vidon, Philippe. (2012). Towards a better understanding of riparian zone water table response to precipitation: surface water infiltration, hillslope contribution or pressure wave processes. Hydrological Processes.21, 3207–3215.

Xu, Y., Shen, Y., & Wu, Z. (2013). Spatial and temporal variations of land surface temperature over the Tibetan Plateau based on harmonic analysis. Mountain Research and Development, 33(1), 85-94.

Zawawi, M. H., Syafalni, A. I., Rahman, M. T. A., Hashim, M. M. M., & Abdullah, R. (2014). Integrated Pollutant Fingerprinting of Shallow Groundwater using Resistivity Imaging Profiling and Hydrochemical Methods at the Beriah Landfill Site. International Journal of Applied Environmental Sciences, 9(4), 2161-2173.

APPENDIX A. Remote sensing output of NDVI, LST, SMOS, and RBC

1- Remote sensing data: output of NDVI throughout the study area covering period (2009 to 2018) extracted by using Cell statistic tools.

A- Mean of the NDVI

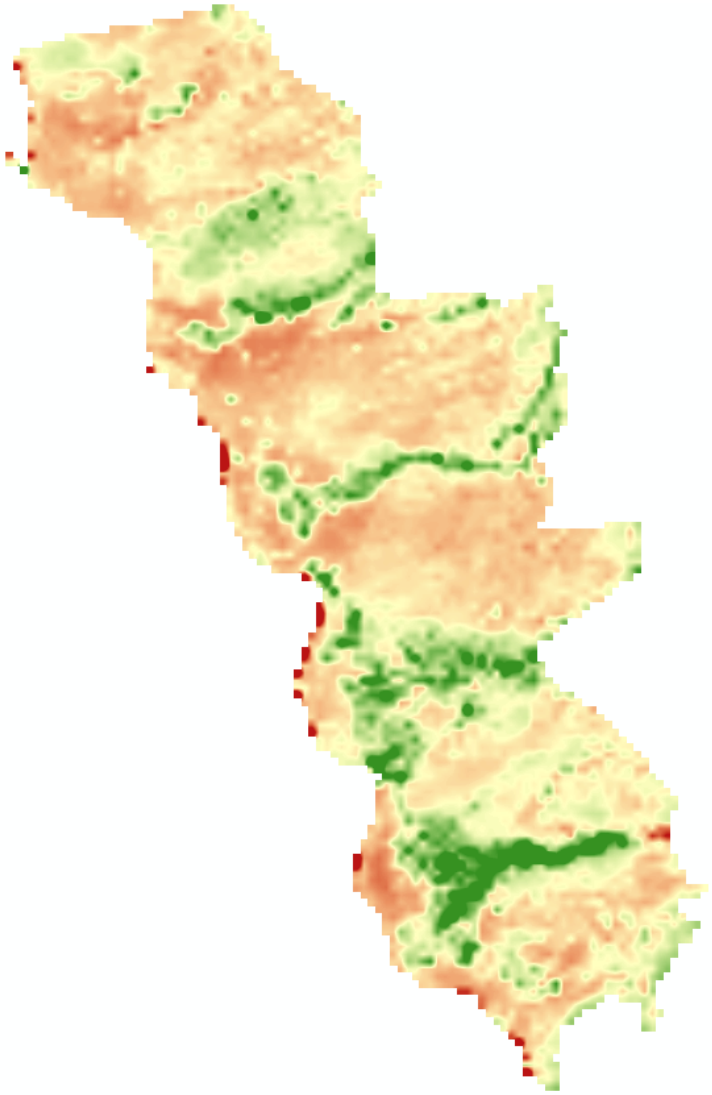

B- STD of the NDVI

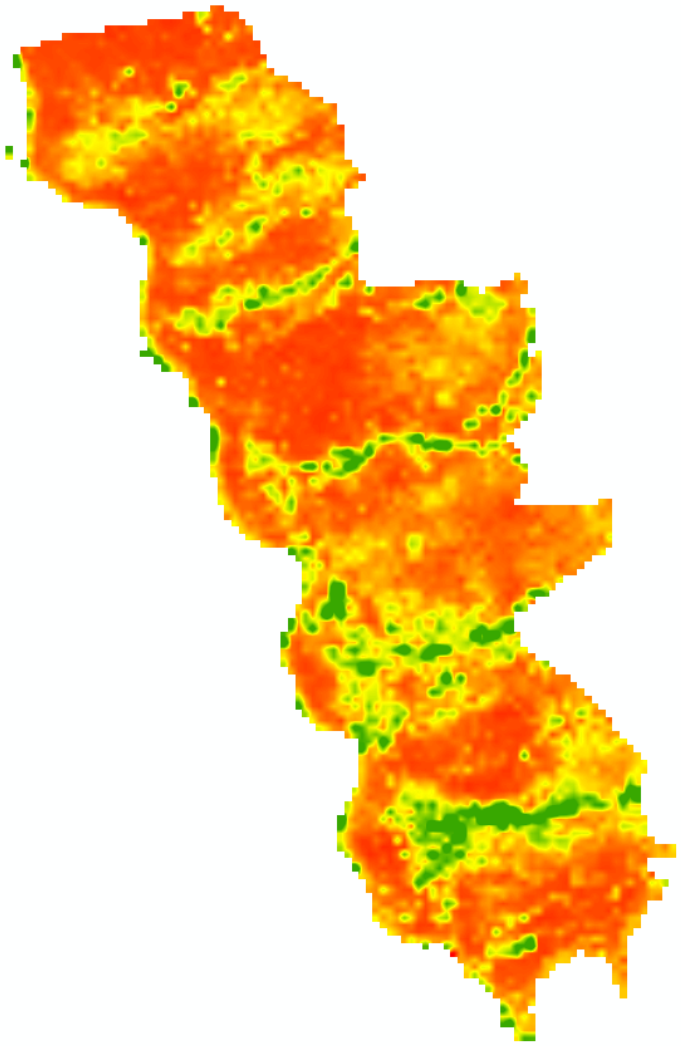

C- Maximum of the NDVI

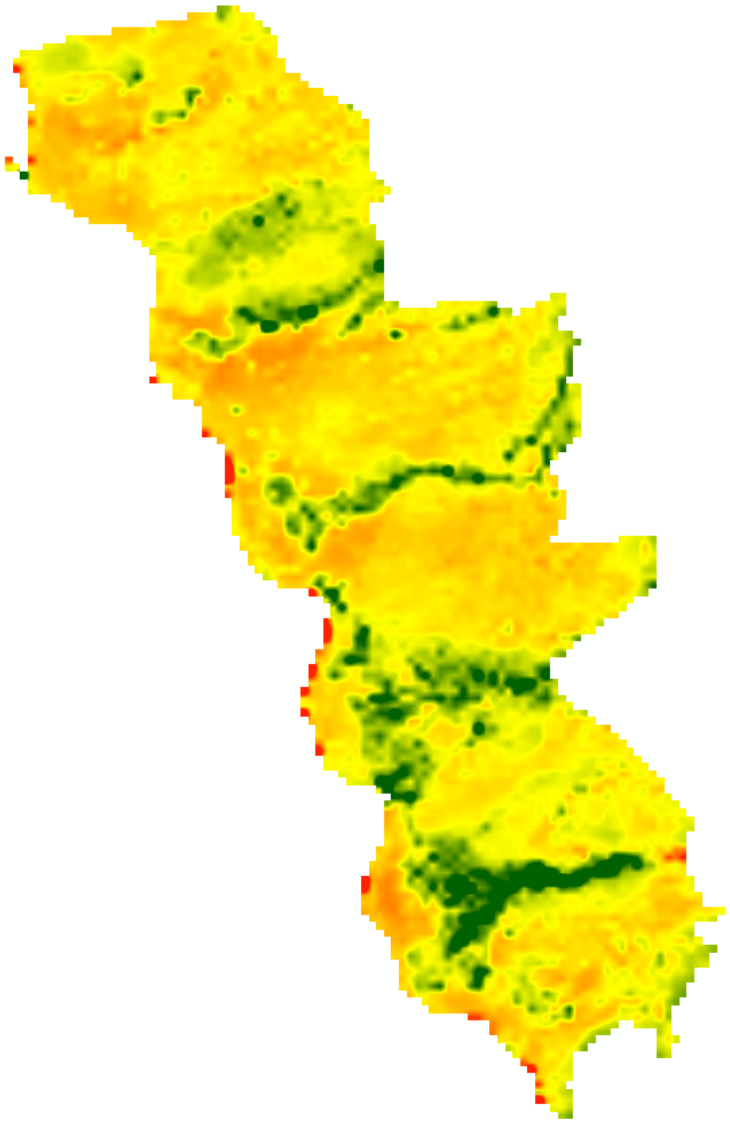

A- Minimum of the NDVI

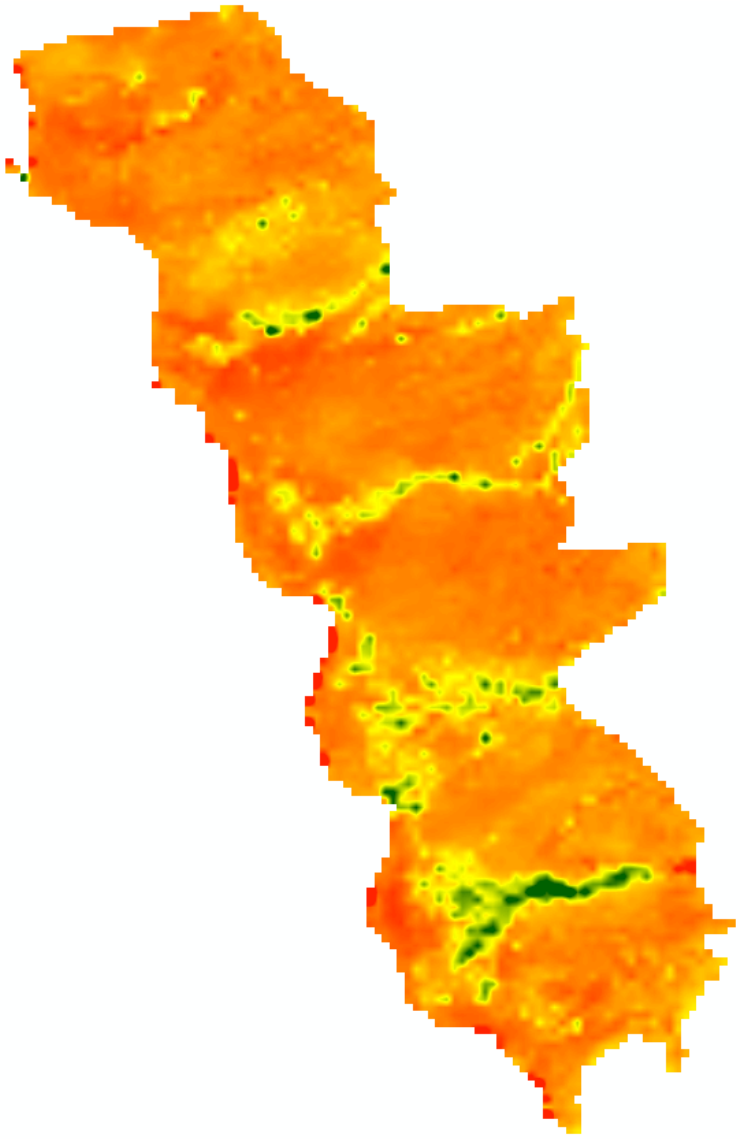

2- Remote sensing data: Output of LST throughout the study area covering period (2009 to 2018) extracted by using Cell statistic tools.

A- Mean of the LST

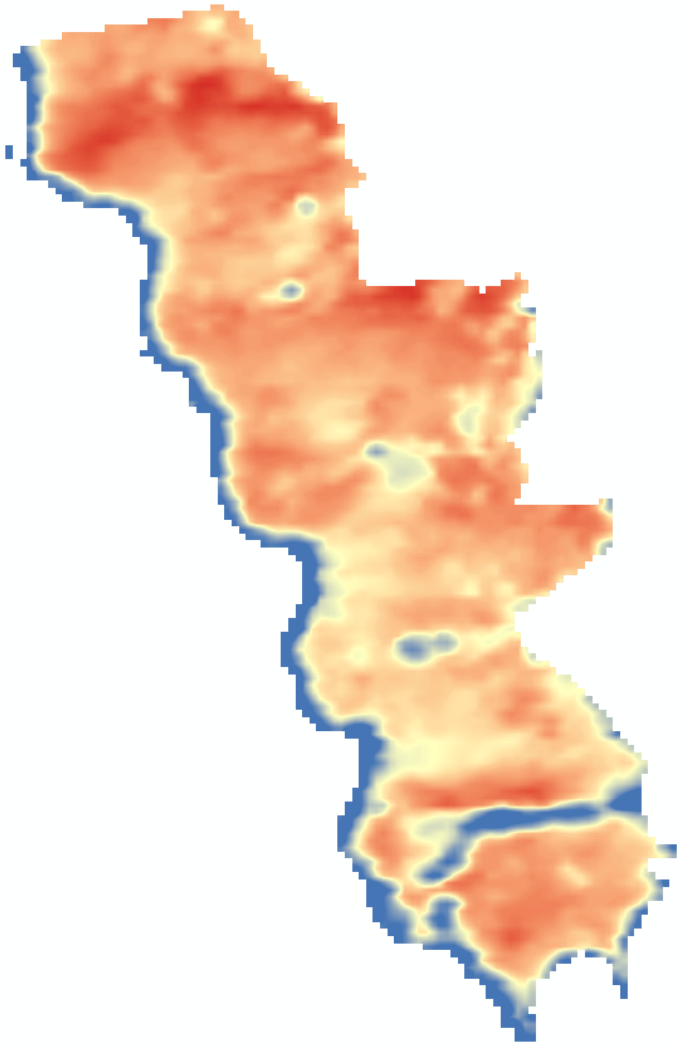

B- STD of the LST

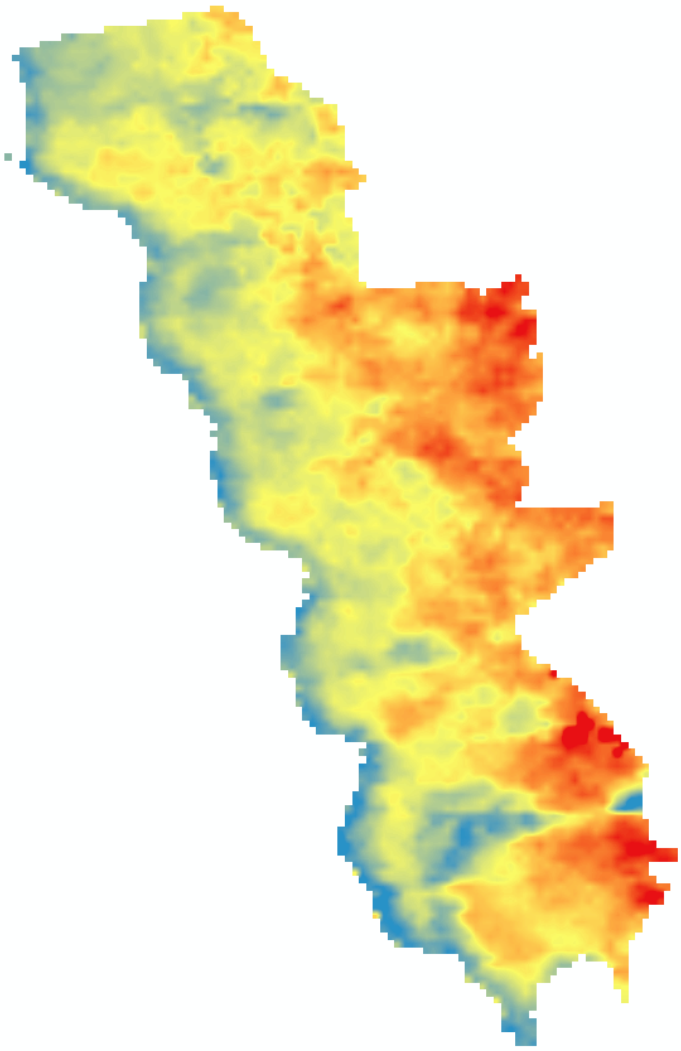

C- Maximum of the LST

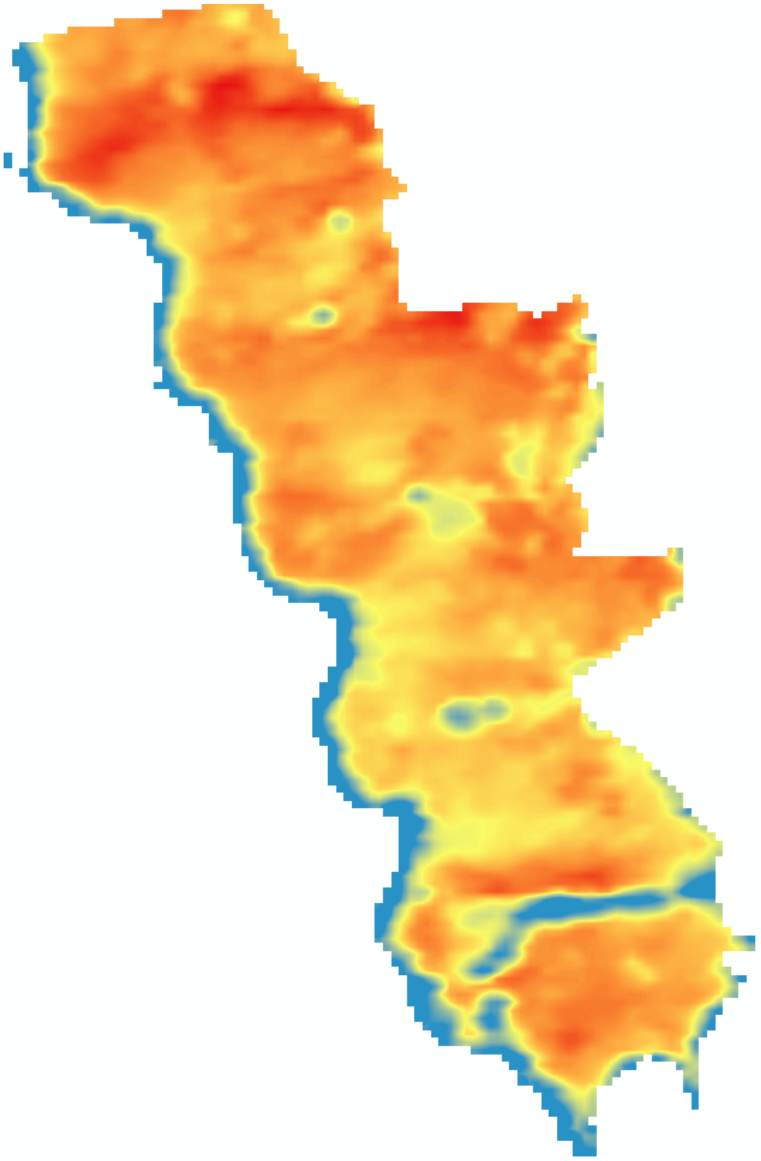

D- Minimum of the LST

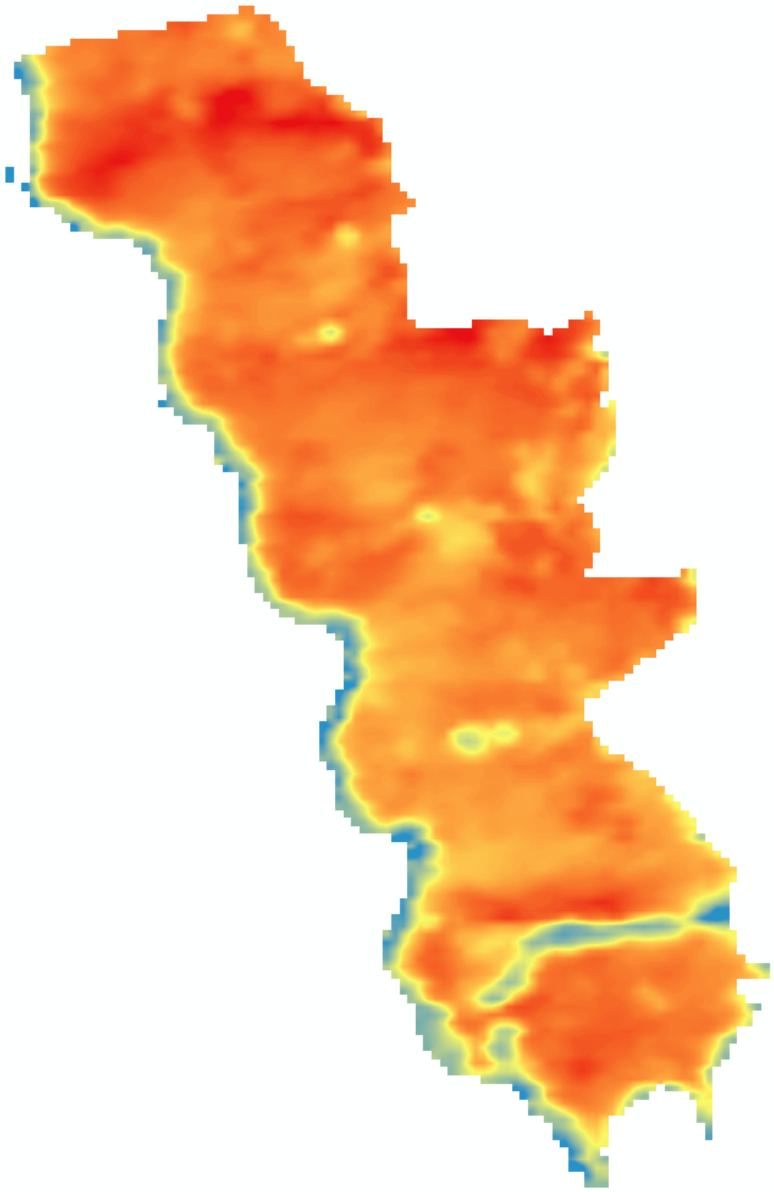

3- Remote sensing data: Output of radar backscattering coefficients RBC throughout the study area covering period (2015 to 2018) extracted by using Cell statistic tools.

A- Mean of the RBC

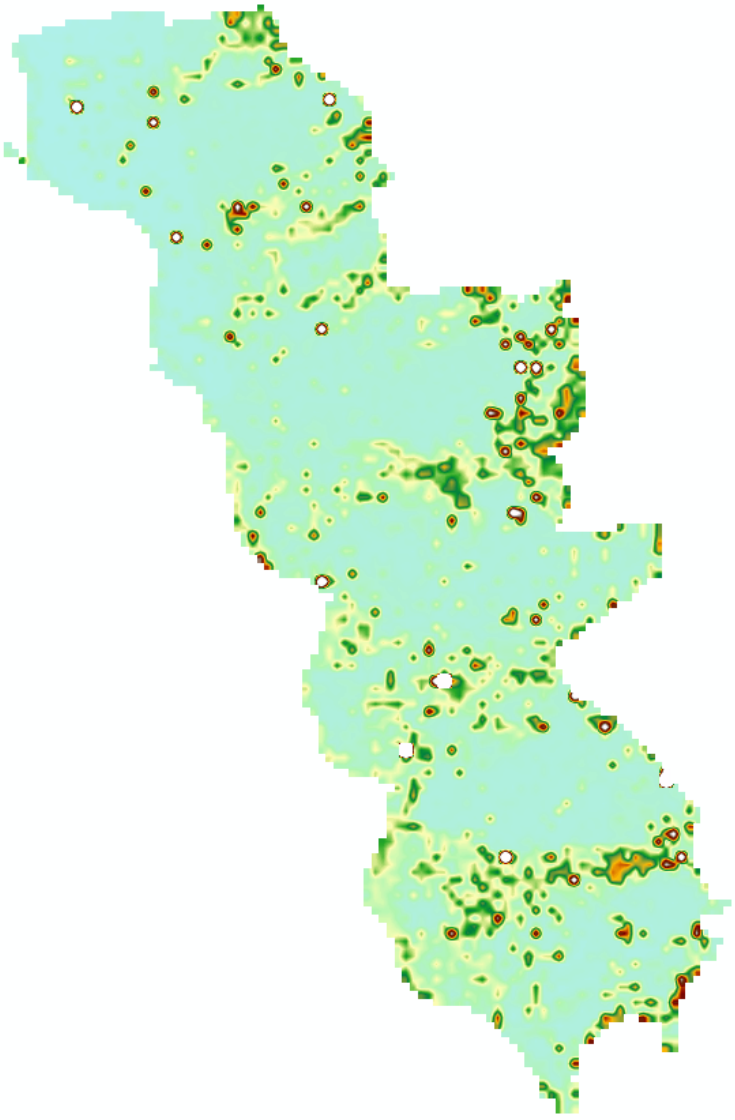

B- STD of the RBC

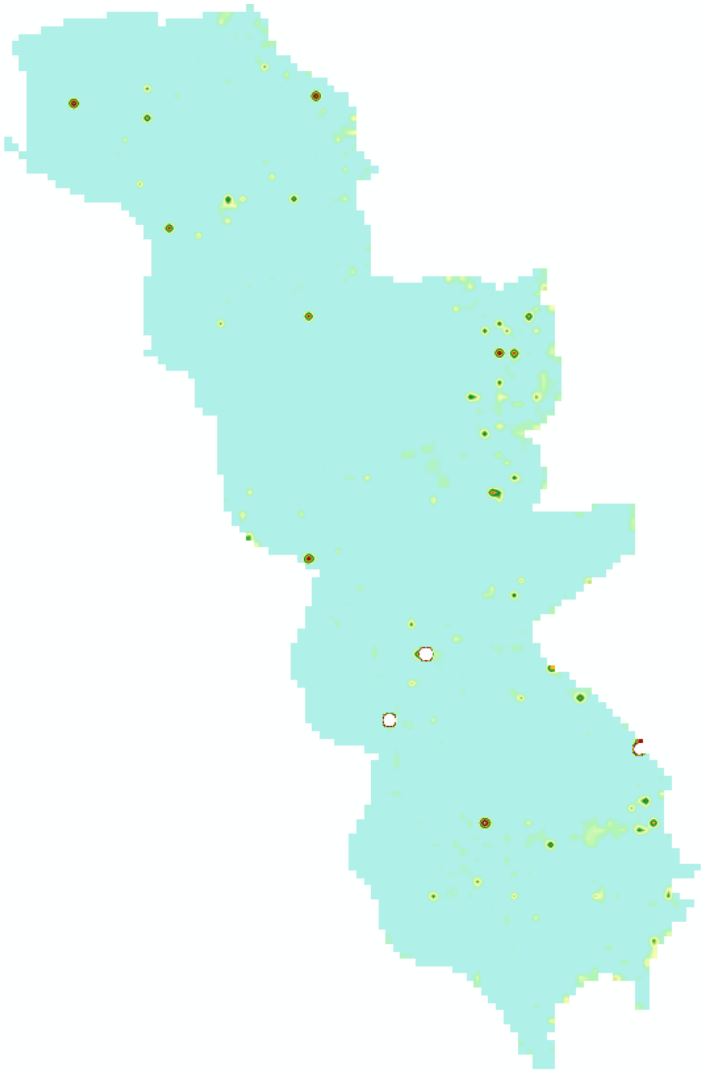

C- Maximum of the RBC

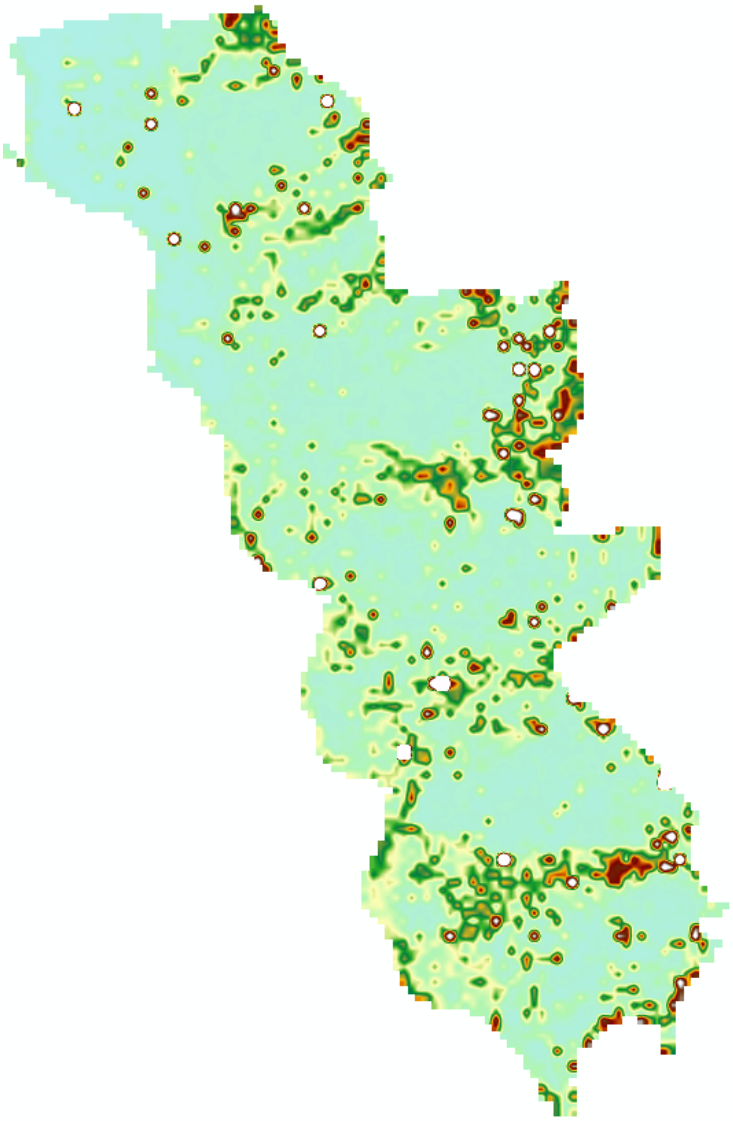

D- Minimum of the RBC

4- Remote sensing data: Output of SMOS throughout the study area covering period (2010 to 2018) extracted by using Cell statistic tools.

A- Mean of SMOS

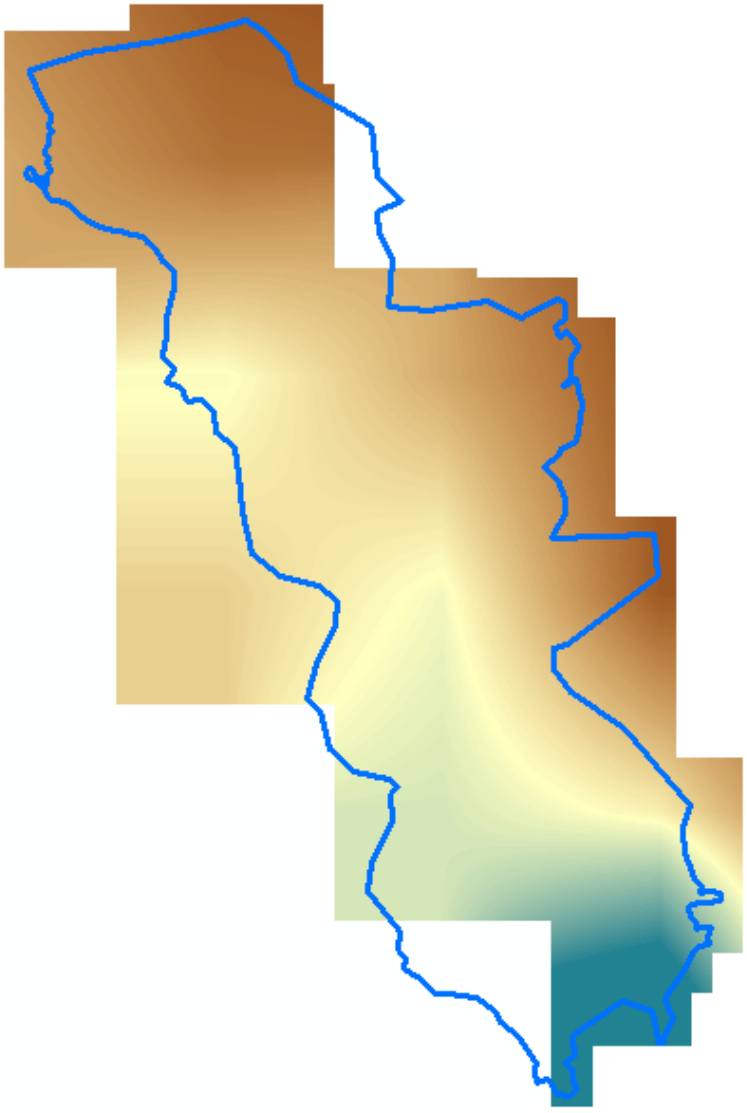

B- STD of SMOS

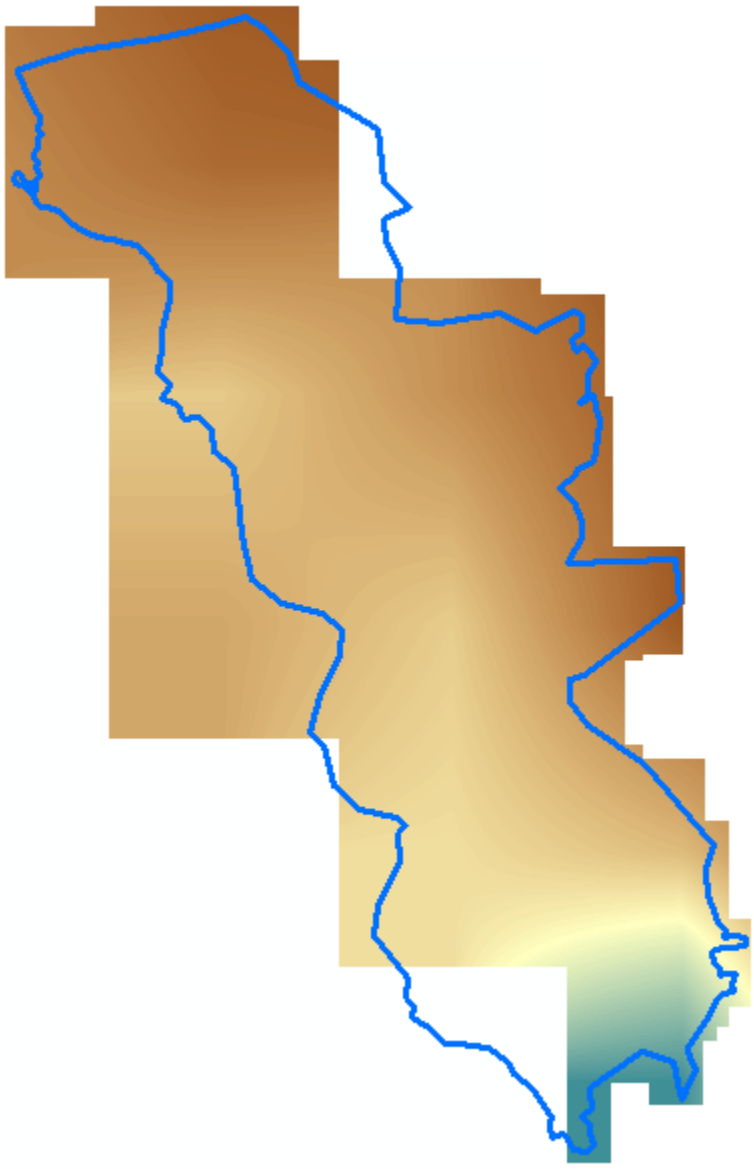

C- Maximum of SMOS

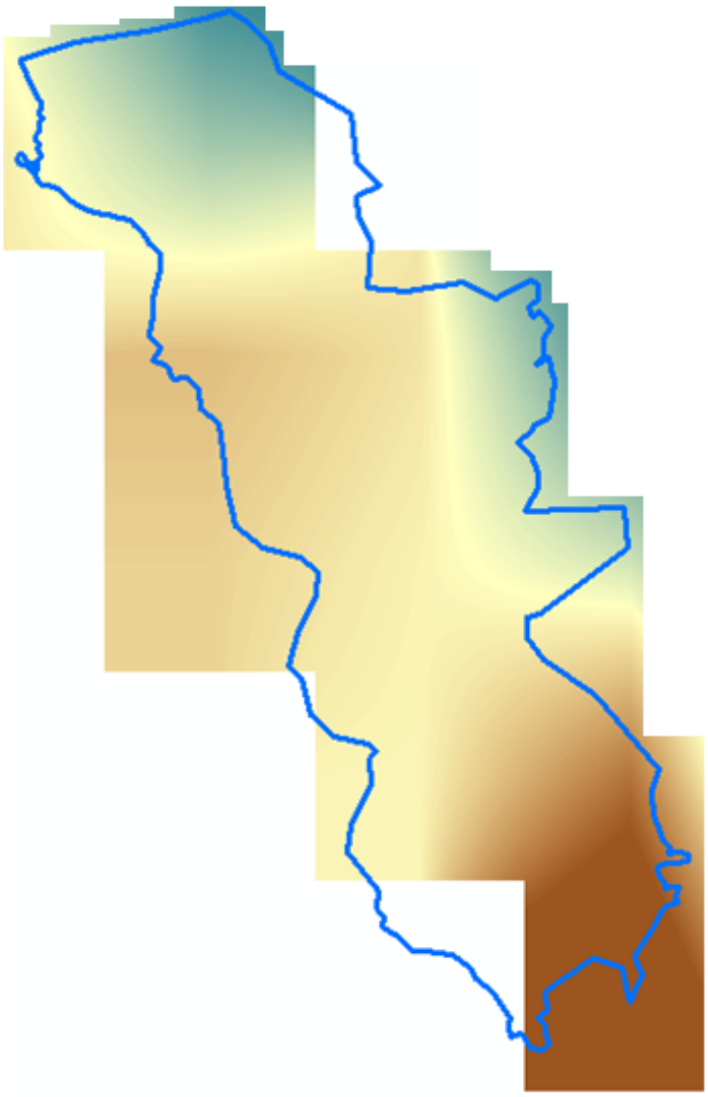

D- Minimum of SMOS

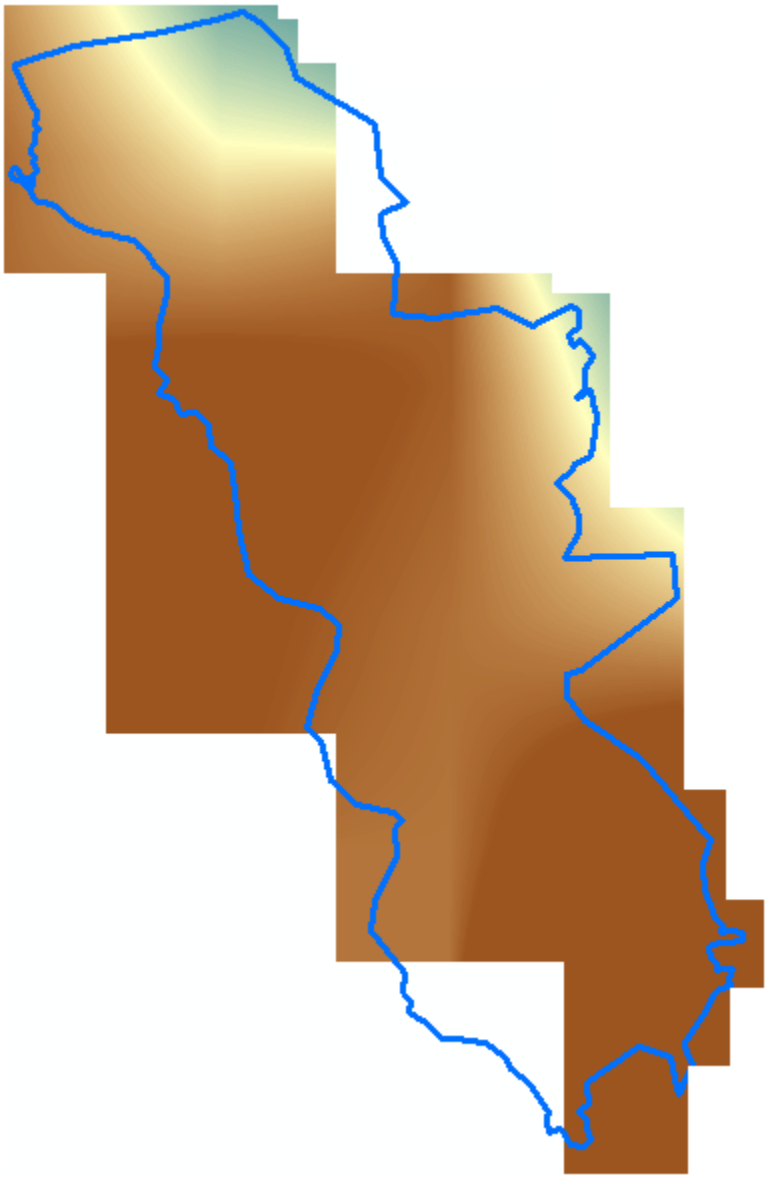

APPENDIX B. Maps of the Study area

A- Map of Al Qunfudah city and its surrounding

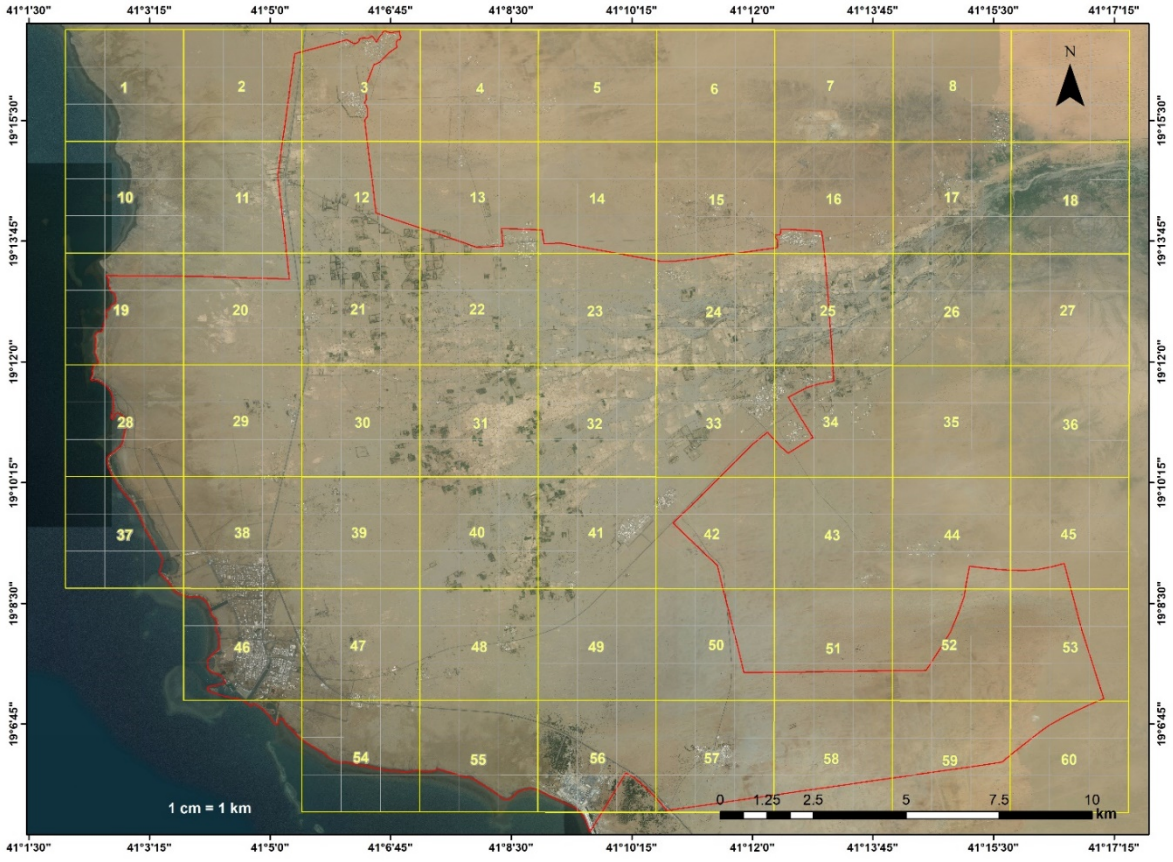

B- The distribution of electric conductivity in groundwater

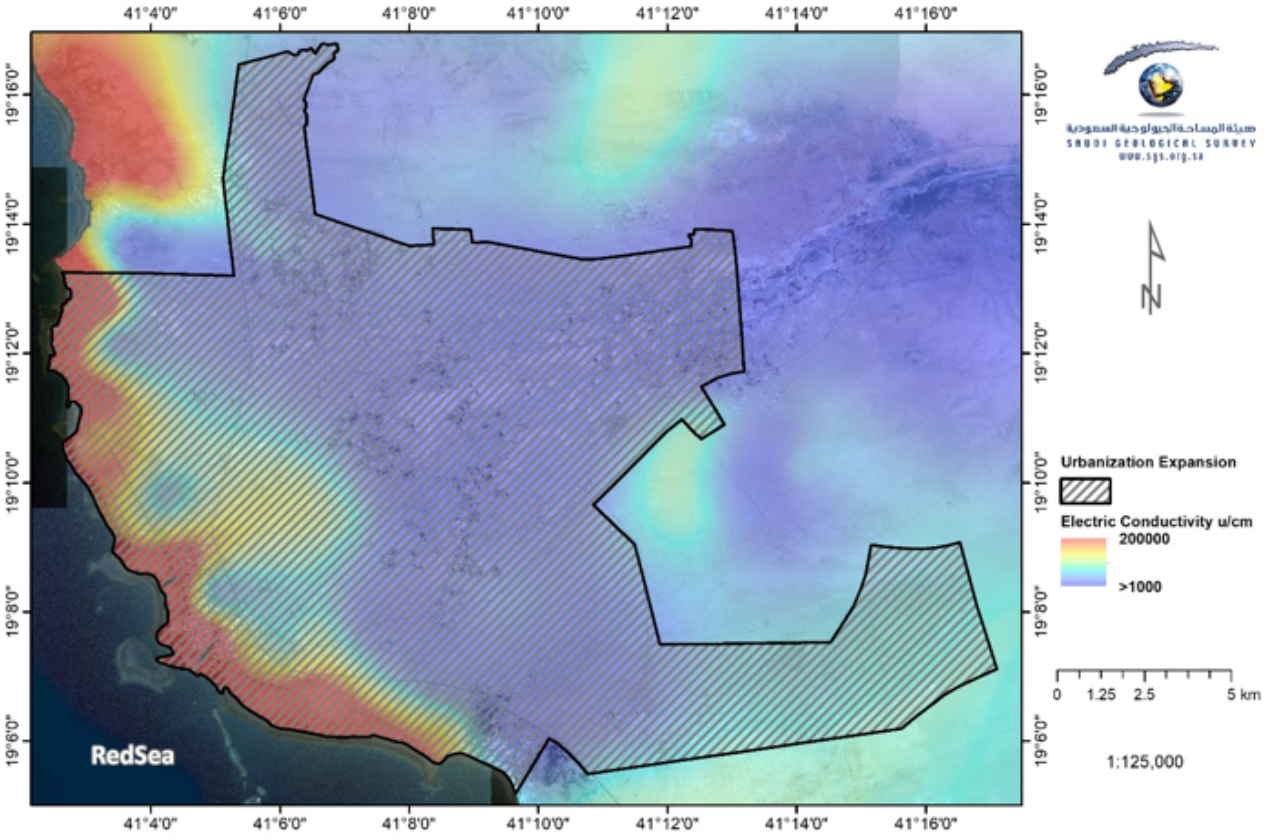

C- The distribution of the wells location in Al Qunfudah city and its surroundings.

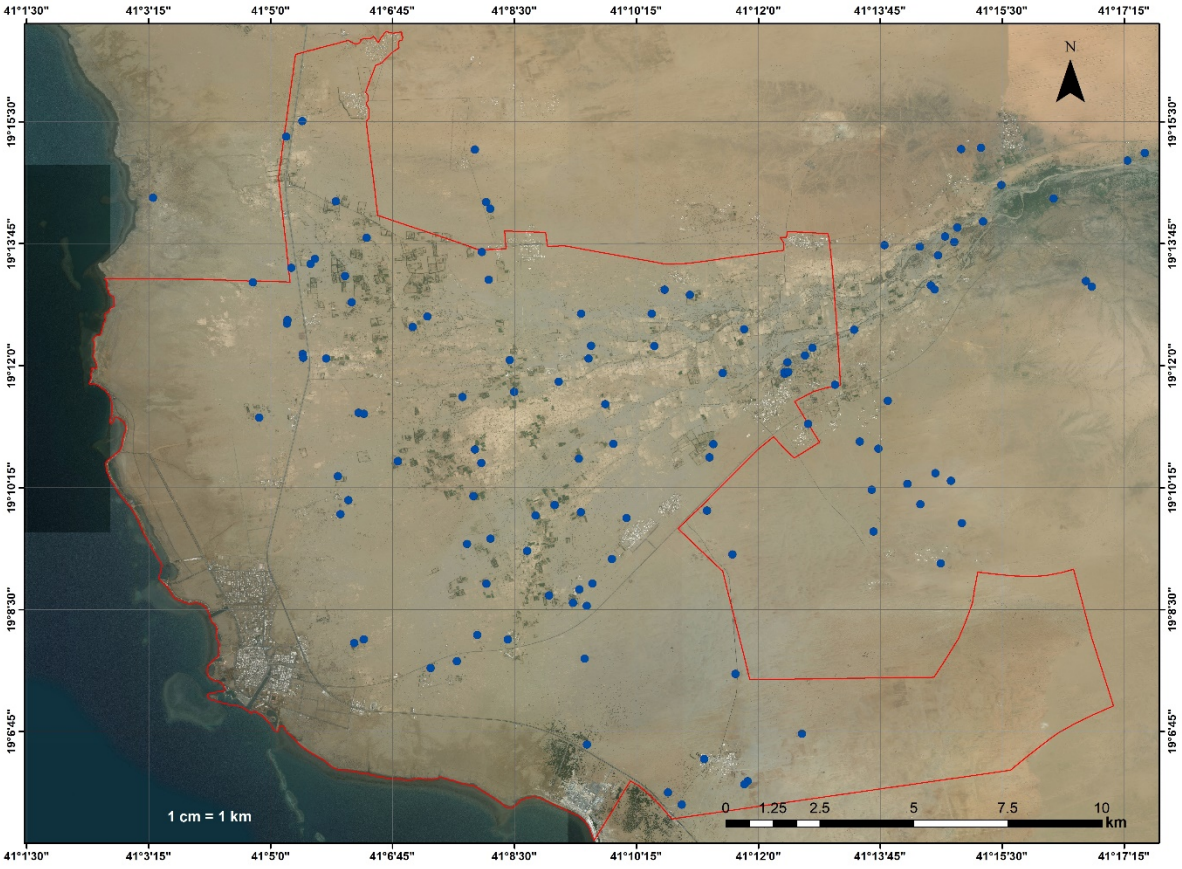

APPENDIX C. Geological maps of Al Qunfudah Province provided by SGS

A- Geological map for Al Qunfudah Province.

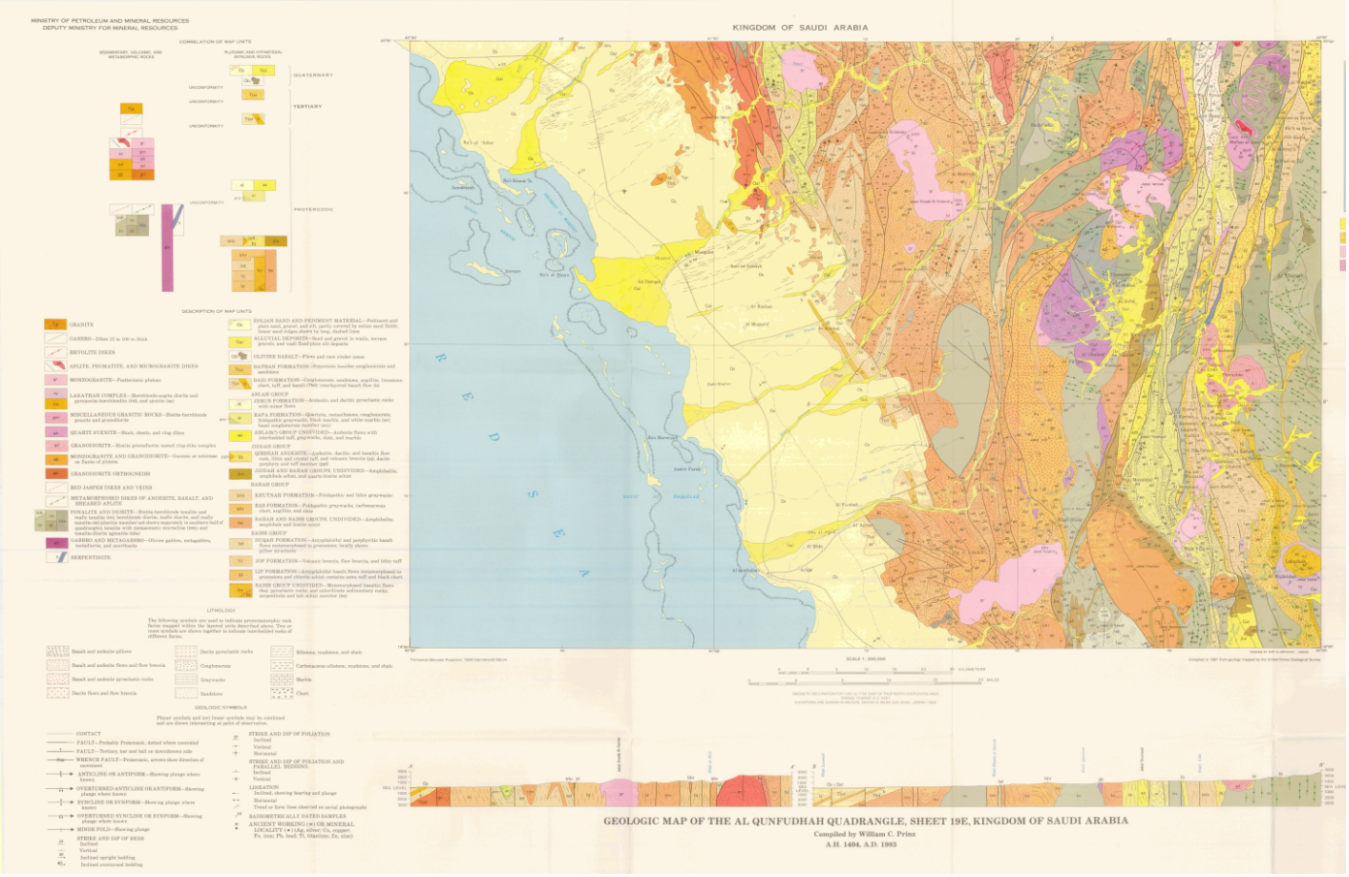

B- Geological map for Al Qunfudah City.

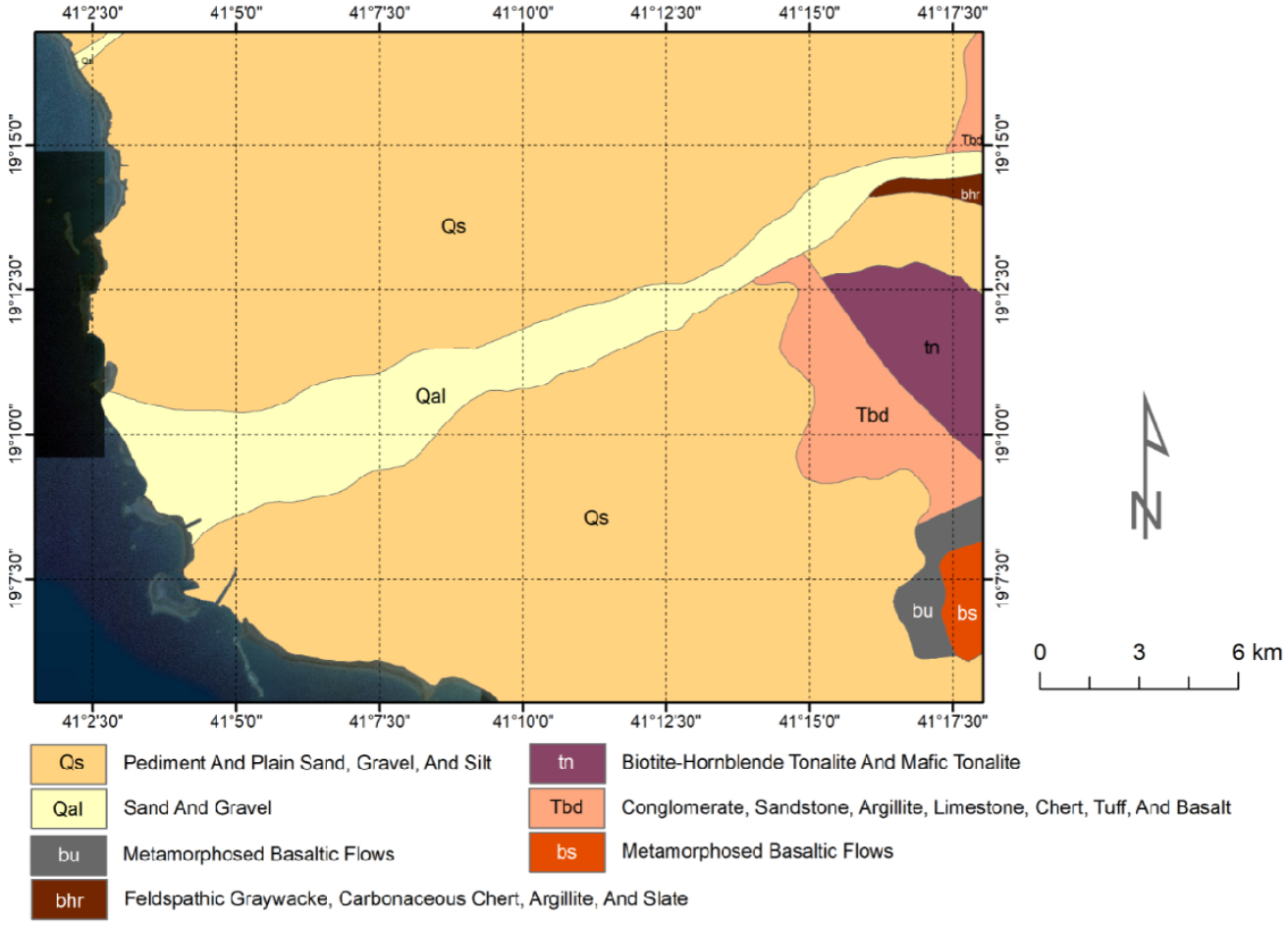

C- Structural sketch map scale 1: 1 000 000 (Saudi Geological Survey)